PAPER AAS 91-501

MARS ENTRY-TO-LANDING TRAJECTORY OPTIMIZATION AND CLOSED LOOP GUIDANCE

Marc R. Ilgen, Raymund A. Manning and Manuel I. Cruz
TRW Space & Technology Group
Redondo Beach, CA

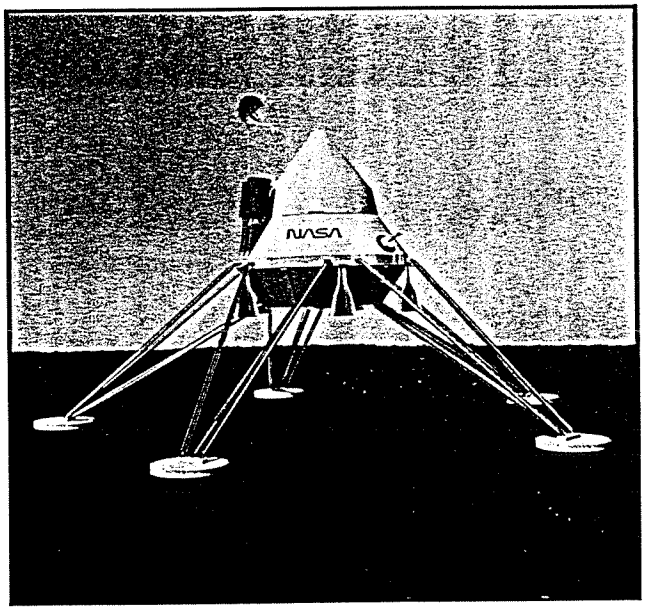

AAS/AIAA Astrodynamics Specialist Conference

Durango, Colorado August 19-22, 1991
AAS Publications Office, P.O. Box 28130, San Diego CA 92128

MARS ENTRY-TO-LANDING TRAJECTORY OPTIMIZATION AND CLOSED LOOP GUIDANCE

Marc R. Ilgen*, Raymund A. Manning**, and Manuel I. Cruz***

This paper addresses Mars entry-to-landing trajectory optimization and closed loop guidance strategies. The phases considered include the initial entry phase, the terminal aerodynamic deceleration phase and the final propulsive soft landing phase. The paper discusses options and tradeoffs for both ballistic and aeromaneuvering entry to a landing site. It also discusses terminal descent guidance strategy optimization and performance. The parameters used to quantify performance are those associated with the Mars Rover Sample Return (MRSR) Phase A studies conducted by TRW.

INTRODUCTION

The primary objective of the Mars Rover Sample Return (MRSR) mission is to return samples from the Mars surface for detailed study in Earth laboratories. In order to accomplish this objective it is necessary for the MRSR landing vehicle to land autonomously on the planet surface. The entry-to-landing trajectory is divided into three phases: initial entry from low Mars orbit, aerodynamic deceleration, and terminal descent. Each of these phases is discussed in detail below.

The Mars entry phase begins with the lander being in the orbit achieved as a result of aerocapture (see Figure 1 and Reference 1). A deboost burn is performed to target the vehicle to enter the Mars atmosphere at a specified flight path angle. The aerodynamic deceleration phase begins after atmospheric entrance (defined to be an altitude of 125 km) down to an altitude of approximately 10 km, where the terminal descent phase for soft landing starts. Figure 2 shows the Mars entry phases.

Two options were considered for the Mars entry and aerodynamic deceleration phases: aeromaneuver and aerobrake. For aeromaneuver, the lander enters the atmosphere and flies along a specified drag trajectory using much the same guidance and control algorithms as were used for aerocapture. For this option, the aeroshell used for aerocapture is reused for entry. For aerobrake, the aeroshell is ejected and rides on a high drag device known as an aerobrake. The lander is attached to the aerobrake, enters the atmosphere, and flies an uncontrolled ballistic trajectory, decelerating quickly until an altitude of 10 km is reached. At this point, the lander is travelling nearly vertically with a descent velocity of 100 to 120 m/s. The aerobrake is ejected and the terminal descent phase begins.

*Senior Member of Technical Staff, Engineering and Test Division, TRW Space and Technology Group, AIAA member
**Staff Engineer, Engineering and Test Division, TRW Space and Technology Group, AIAA member
***Senior Systems Engineer, Federal Systems Division, TRW Space and Technology Group, AIAA member

The aerobrake option was chosen as the baseline option for Mars entry and aerodynamic deceleration. The trades justifying this choice will be discussed. The aeromaneuver entry trajectory analysis and the aerobrake entry and terminal aerodynamic deceleration analysis will also be discussed in detail.

The terminal descent phase begins at an altitude of approximately 10 km and lasts until a soft landing has been achieved. The desired landing site is determined *a priori* from orbit (pinpoint landing scenario) or concurrently with terminal descent (hazard avoidance scenario). For either of these scenarios, the lander uses an explicit guidance strategy to maneuver to the desired landing site. The guidance strategy is a robust derivative of E-Guidance [2] and is presented in detail in this paper.

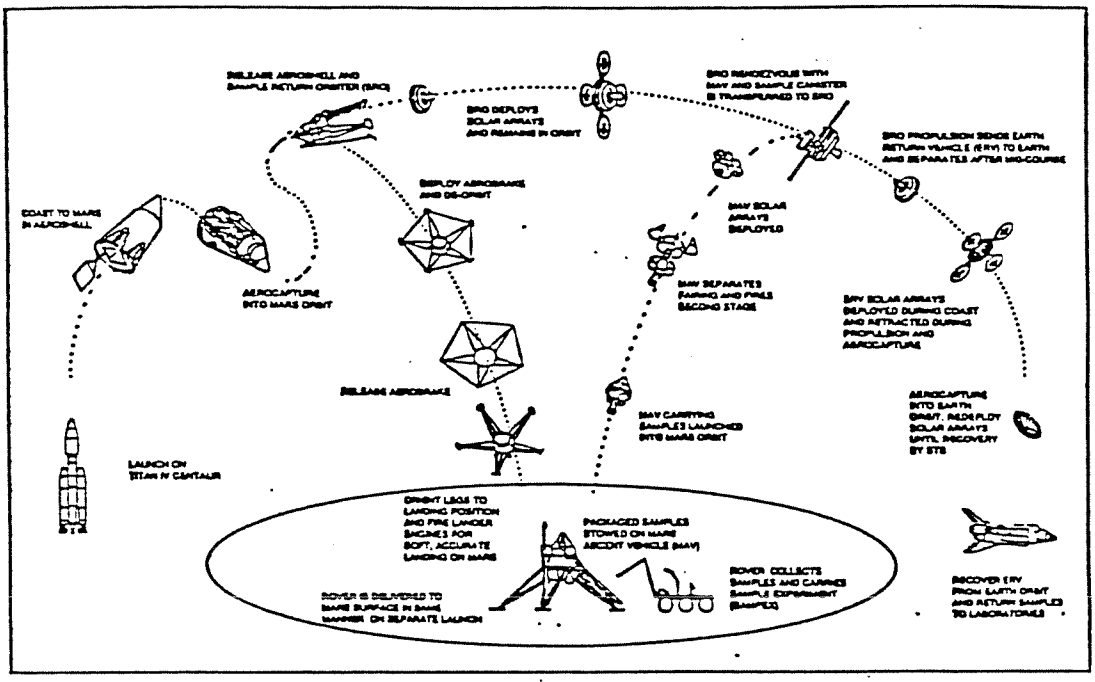

Figure 1. MRSR Mission Sequence

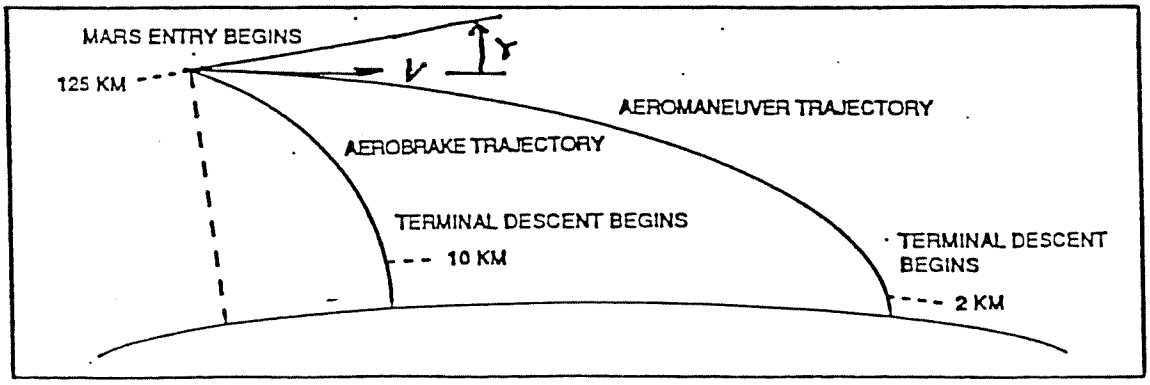

Figure 2. Mars Entry Phases

INITIAL ENTRY PHASE ANALYSIS

In the baseline mission, the aerocapture orbit is a 500 x 1500 km orbit. Estimates were made for the ΔV required to enter at the prescribed vacuum periapsis or entry flight path angle, as well as for the partial derivatives describing the sensitivity of delivery accuracy to the deorbit maneuver. Figures 3 through 6 present plots of deorbit ΔV, the vacuum periapsis radius, the partial derivative ($\partial\gamma_E/\partial\Delta V$) of the entry flight path angle to deorbit ΔV, and the partial derivative ($\partial\gamma_E/\partial r_p$) of the entry flight path angle to the vacuum periapsis, all as functions of the entry flight path angle. It will be shown below that the entry flight path angles required for the aeromaneuvering and aerobrake options are -3.75 degrees and -15 degrees, respectively. As such, the required deorbit ΔVs are about 100 m/s for the aeromaneuvering option and 260 m/s for the aerobrake option.

The requirements for this study state that the planet relative position shall be known to a 1-km accuracy or better. All error analyses presented here use this requirement to estimate landing accuracy.

AEROMANEUVER VERSUS AEROBRAKE TRADES

The aeromaneuver and aerobrake descent options were compared to assess their relative performance. Table 1 shows the results of this comparison in terms of key requirements. Both options can satisfy the stated requirements. However, the aerobrake option performance exceeds the requirements when compared to the aeromaneuvering option. For this reason, the aerobrake option was chosen as the baseline option for Mars entry.

The key performance parameters in the comparison were system mass, terminal descent conditions, landing accuracy, and thermal control. The following paragraphs present details of the comparisons between the two options for each of these parameters.

Mass Required. The system masses required at launch for the aeromaneuvering and aerobrake options are 6070 kg and 5725 kg, respectively. The aerobrake mass requirements are lower because:

1) The aerobrake capitalizes on the lander legs for support structure and the mass for the fabric is offset by eliminating the parachute.
2) Since the aeroshell is jettisoned after aerocapture, the propellant required to raise periapsis after aerocapture is decreased.
3) The aeroshell bondline for aerocapture is designed for a shorter soak-through time because the aeroshell is jettisoned after aerocapture.
4) Since the spacecraft can thermally radiate to space shortly after aerocapture, the thermal mass required to isolate the spacecraft from the aerocapture and internal thermal loads (i.e., RTGs) is less.

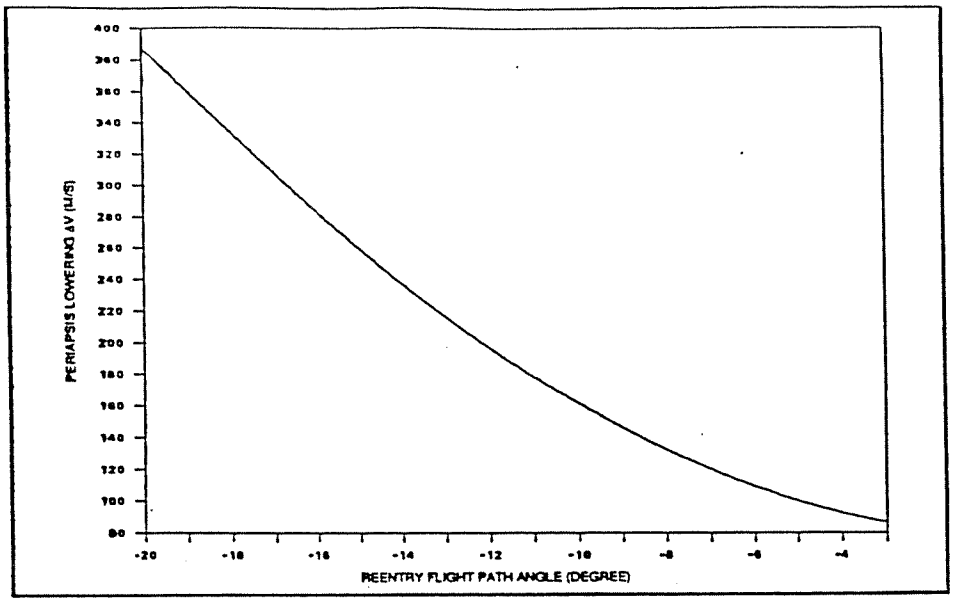

Figure 3. Reentry ΔV Versus Entry Flight Path Angle

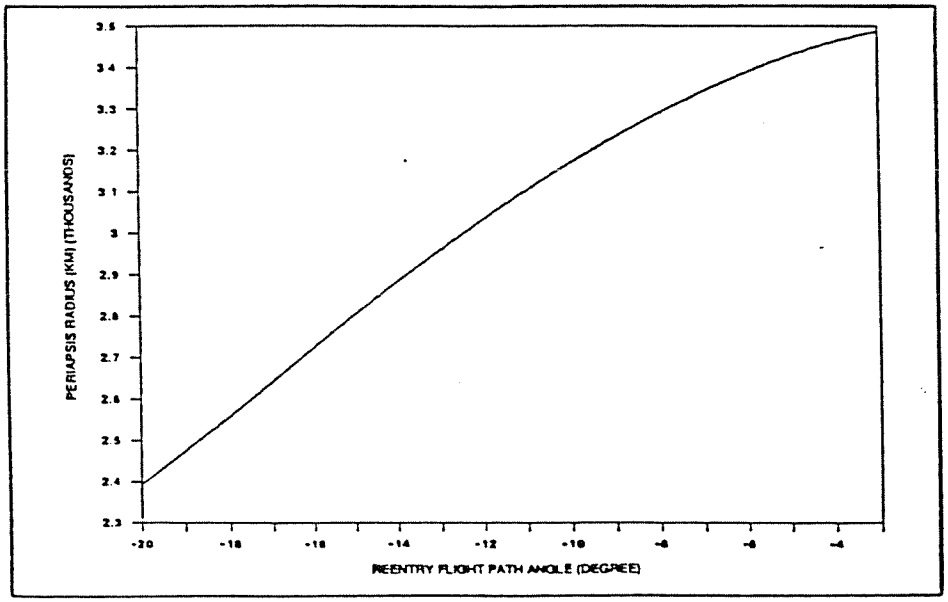

Figure 4. Periapsis Radius Versus Entry Flight Path Angle

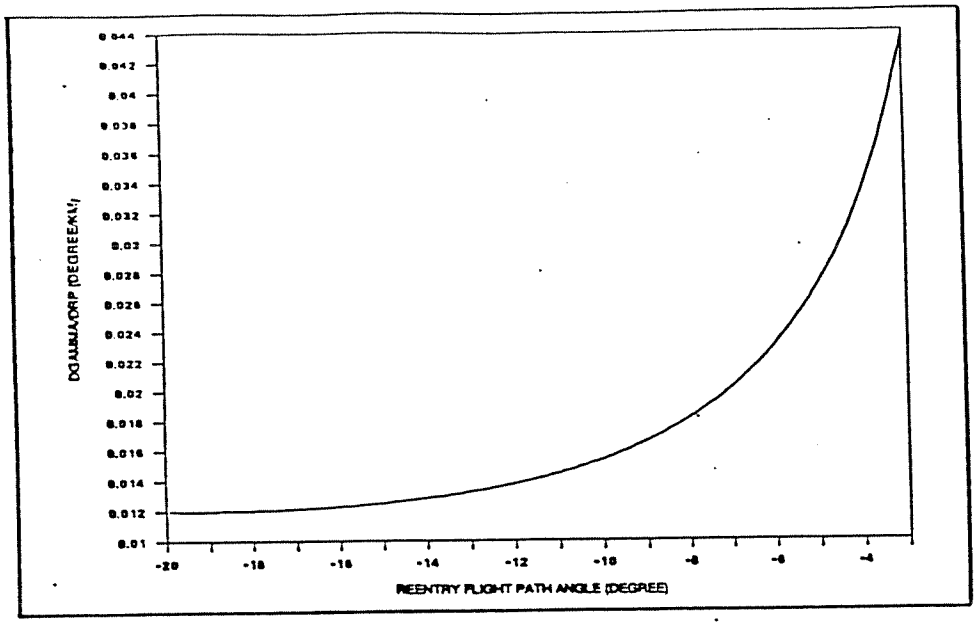

Figure 5. $\partial\gamma_E/\partial r_p$ Versus Entry Flight Path Angle

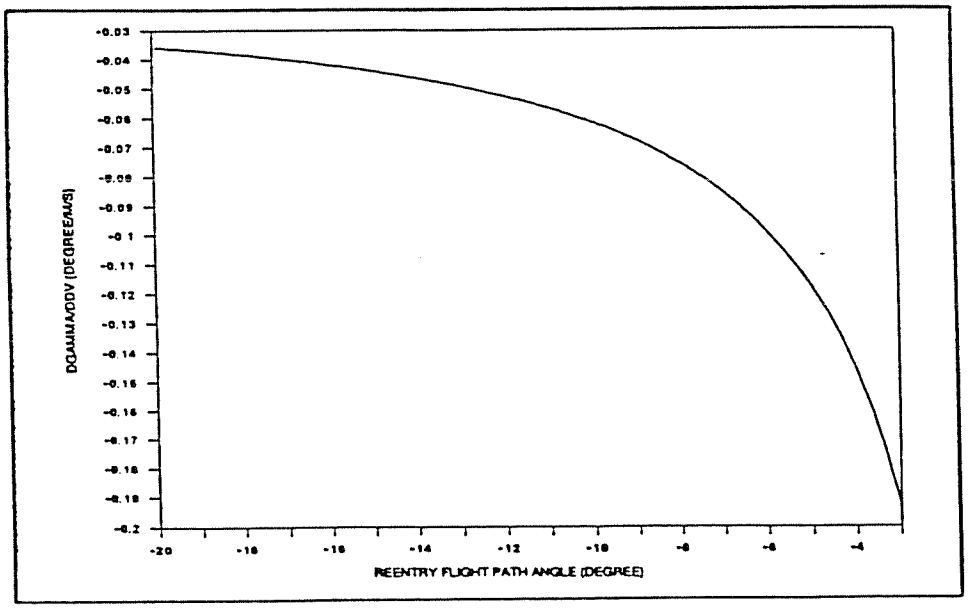

Figure 6. $\partial\gamma_E/\partial\Delta V$ Versus Entry Flight Path Angle

5) It is shown below that the aerobrake option requires a steeper entry flight path angle than the aeromaneuver option does (-15 degrees as compared to -4 degrees). As a result, the ΔV required to lower periapsis for entry-to-landing is larger for the aerobrake option. However, the aerobrake option delivers a lower mass to the entry interface since this option does not carry the aeroshell down to the entry interface (the aeroshell is jettisoned after aerocapture). The higher ΔV requirement is offset by the lower mass the ΔV is required to move, and the fuel mass requirements for the deboost maneuver are approximately equal for the two options.

Table 1. Entry and Landing Concepts Comparison

Requirement	Biconic Reuse	Aerobrake
Demonstrate aerobraking technologies for a manned mission	Demonstrate aeromaneuver biconic	Supplements aerocapture biconic demonstration
Launch mass	Minimum mass solution when compared to an all propulsive mission	Lower mass requirement when compared to aeroshell reuse
Thermal control during and after aerocapture thermal soak through	Thermal fluid loop control to reject RTG, aerothermo soak through and other subsystem thermal loads	No thermal control required; thermal radiation out to space; aeroshell jettisoned after aerocapture
Thermal control during entry to landing	Thermal fluid loop control to reject RTG, aerothermo soak through and other subsystem thermal loads	No thermal control required; thermal radiation out to space; aeroshell jettisoned after aerocapture
Allow for terminal area deceleration for a propulsive soft landing	Parachute deployment at a sufficiently high altitude to limit loads and terminal sequence of events to soft landing	Aerobrake in a near terminal descent trajectory at 10-km altitude with about a 100 m/s descent rate; parachute not required
+3 km and -2 km altitudes for the target site	Can be met	Consider altitudes between +8 to +10 km
Reach targets for the RL within a 10 x 10 km area and for the SRL within a 100 x 100 m area	Aeromaneuver (approx. 1000 sec) into the proximity of the target area, perform low altitude (approx. 1 km) target area relative position measurements at high rate and propulsively soft land	Enter in a steep ballistic mode with load error propagation (approx. 150 sec), acquire landing site at high altitudes (approx. 10 km) over target area, and propulsively maneuver to a target site soft landing
Allow for the terminal descent landmark and acquisition by a variety of sensor spectral ranges	Can be met; certain sensor spectral ranges may be limited to different phases depending on aeroshell transparency and pointing requirements while on the parachute and/or propulsion	With a near terminal descent over the target area (≤10 x 10 km) at an altitude of 10 km, can be readily met for a wide sensor spectral range

Furthermore the aeromaneuvering option imposed a conflicting aerodynamic requirement with aerocapture. Aerocapture usually requires flight at maximum Lift-to-Drag ratio(L/D_{max}) for maximum flight path controllability whereas aeromaneuvering requires flight at maximum Lift coefficient($C_{L_{max}}$) to minimize the ballistic coefficient B ($=m/C_DA$). The lowest possible ballistic coefficient is needed to keep the thermal protection mass requirements as low as possible. The aeromaneuver option is not as mass efficient as the aerobrake option because additional mass is required for the aeromaneuver option to overcome its relative incompatibility with aerocapture.

Terminal Descent Conditions. To effect an accurate, safe, and soft landing, it is required that the lander be in a near-terminal state at a sufficiently high altitude to acquire the perspective target landing site and to propulsively maneuver to that site in a fuel-optimal manner. The aeromaneuvering option reuses the aeroshell; therefore, the ballistic coefficient is constrained to that required for aerocapture. With the current lander mass estimates, the ballistic coefficient is such that the parachute deployment for lander egress and terminal descent requires the altitude to be on the order of 6 km for Mach 2 to 3 deployment. This results in a limited amount of time for the landing site acquisition to take place. Because parachute deployment takes place at a low altitude, a certain amount of time is required to damp the parachute deployment induced angular motion. Near terminal conditions are not reached until the lander has descended as low as 2 km. On the other hand, the aerobrake achieves a near-terminal state at about 10-km altitude. This altitude allows much more time for landing site acquisition.

Landing Accuracy. The landing accuracy requirement is 10 x 10 km, which is equivalent to a circular error probable (CEP - 3 sigma) of 7 km. The aeromaneuvering option has a projected CEP of 6 km. The aerobrake option CEP is 3 km. The greater accuracy (smaller CEP miss) of the aerobrake option is due to the much shorter flight time, since the a shorter flight time allows much less time over which uncertain disturbances can alter the descent trajectory. Further details of these projections are presented later in the aerobrake and aeromaneuver performance analysis sections.

AEROBRAKE ANALYSIS

The following analyses on the aerobrake reflect the simplicity of the concept from a mission operations and design perspective. The concept demonstrates much greater flexibility in the performance of the landing sequences.

Targeting

The entry ballistic coefficient (B) of the aerobrake option ranges from 5 to 25 kg/m^2 and allows steep entry at relatively low aerothermal and aerodynamic loading. The aerothermal loads become important since the concept is a flexible and deployable structure that readily integrates into the aerocapture aeroshell. Materials considered are Kevlar and Nomex with reinforcing structural ribs. At a B of 15 kg/m2, this corresponds to an aerobrake of about 11-m diameter for an entry mass of 3000 kg and Drag coefficient(C_D) of 2.0. An aerobrake of this dimension is easily folded within the aerocapture aeroshell [1].

The entry flight path angle sensitivities shown in Table 2 were calculated for a ballistic entry vehicle with a B of 15 kg/m^2. The calculations assumed deorbit from a 500 x 1500 km orbit which results in a 3.5-km/s entry speed at a 125-km altitude. The results show that the entry vehicle is in a 120-m/s terminal descent at a 10-km altitude from the aeroid. Note that the downrange travel decreases significantly with increasing entry flight path angle magnitude. This is depicted graphically in Figure 7. Note that the knee of the curve is a -15 degree entry flight path angle. Also, the peak aerodynamic loads increase with increasing flight path angle magnitude. The requirements for this study state that the aerodynamic loads be 6.5 g's or less, which corresponds to an entry flight path angle of -15 degrees or less (by "less" we mean closer to zero or less negative). For these reasons, -15 degrees was chosen as the nominal entry flight path angle. Finally, note that the peak heating rates are quite low (2 to 4 W/cm^2) for the full range of entry flight path angles considered.

Guidance

The aerobrake does not require an active flight guidance system. It maintains a navigation inertial reference system to aid in issuing the staging command for the aerobrake and lander free fall.

Flight Control

The aerobrake does not require an active flight control system. It will be designed to passively fly at zero angle of attack.

Trajectory Profile

The trajectory profile for the aerobrake nominal entry flight path angle of -15 degrees is shown in Figures 8 through 12. It demonstrates the rapid entry to landing trajectory of the aerobrake compared to the aeromaneuvering trajectory(see Figures 19 through 24). Entry events occur at an order of magnitude faster, thereby preventing the buildup of trajectory dispersions.

Delivery Accuracy

Estimates of the target miss for a steep ballistic entry using an aerobrake with B of 15 kg/m^2 were calculated. Table 3 shows these calculations. The error source magnitudes are representative of previous estimates. For entry at flight path angles of -15 degrees, the target miss estimates are equivalent or better than an aeromaneuvering entry, even though the aerobrake option is a much simpler entry-to-landing approach.

A concern with this concept is the potential existence of high altitude jet streams which might not be compensatable in the entry trajectory. It has been suggested that the jet streams exist primarily at high latitudes of 45 degrees or greater which are outside the range of MRSR landing sites (34°S to 38°N latitudes). In the error analysis, it was assumed that the variability of a jet stream could be estimated to within 10 m/s.

Table 2. Entry Sensitivities to Entry Flight Path Angle

γ-E (deg)	State at 10 km				$\frac{DRG}{d\gamma\text{-}E}$ (km/deg)	q_{max} (nt/m^2)	D_{max} (g's)	Q_{max} (w/cm^2)	Q_{Total} (joule/cm 2)
	γ (deg)	V (m/sec)	T_F (sec)	RG (deg)					
-6	-83	120	468	15.520	191.799	424	2.5	2.2	265
-7	-84	120	423	13.330	129.842	496	2.9	2.5	243
-8	-84	120	388	11.725	95.158	567	3.4	2.7	227
-9	-83	120	360	10.488	73.340	638	3.8	2.8	213
-10	-83	120	338	9.499	58.636	709	4.3	3.0	202
-11	-83	120	318	8.689	48.024	779	4.8	3.2	193
-12	-83	120	302	8.009	40.316	848	5.3	3.3	185
-13	-83	120	287	7.430	34.328	915	5.8	3.4	178
-14	-83	119	274	6.930	29.644	981	6.2	3.6	171
-15	-83	119	262	6.492	25.968	1047	6.5	3.7	166
-16	-82	119	251	6.106	22.886	1111	7.1	3.8	161
-17	-82	119	241	5.762	20.396	1178	7.5	3.9	156
-18	-82	119	232	5.453	18.320	1243	7.9	4.0	152
-19	-82	119	224	5.173	16.600	1307	8.0	4.1	148
-20	-82	119	216	4.919	15.060	1371	8.8	4.3	145
-21	-81	119	209	4.687	13.756	1435	9.3	4.3	142
-22	-81	119	202	4.473	12.688	1496	9.7	4.4	139

γ = Flight path angle

V = Speed

T_F = Time of flight from 125-km altitude

RG = Great circle range angle

$\frac{DRG}{d\gamma\text{-}E}$ = Partial derivative of great circle range to entry flight path angle

q_{max} = Maximum dynamic pressure

Q_{max} = Peak convective heating rate on 1-m sphere

Q_{Total} = Time integral of Q

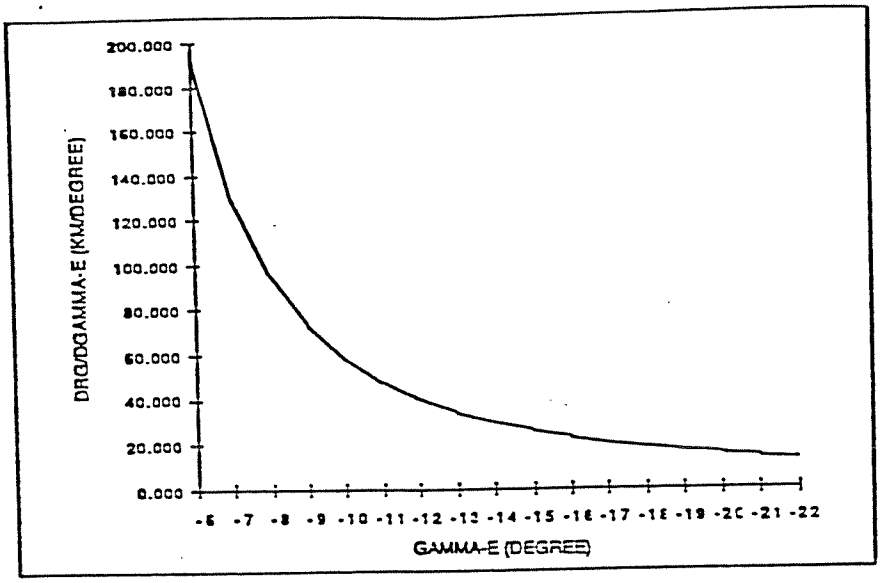

Figure 7. Downrange Sensitivity to Entry Flight Path Angle

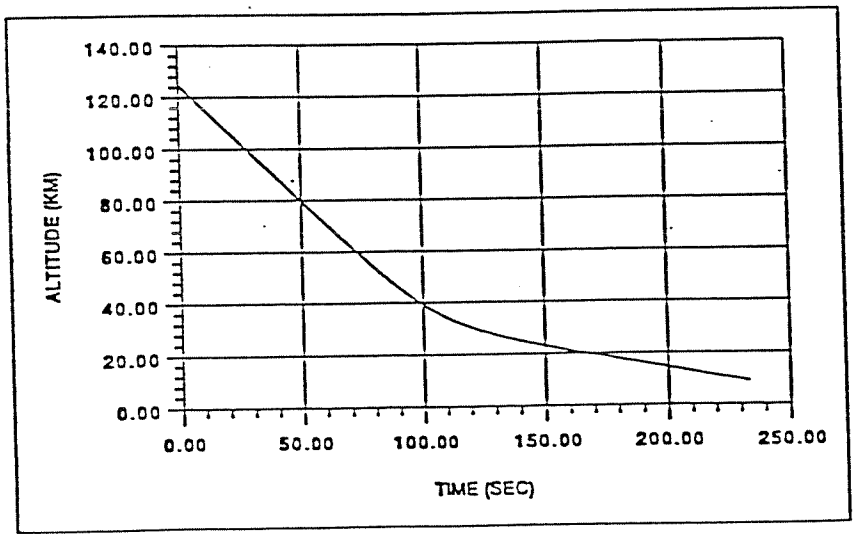

Figure 8. Mars Aerobrake Nominal Trajectory Altitude History

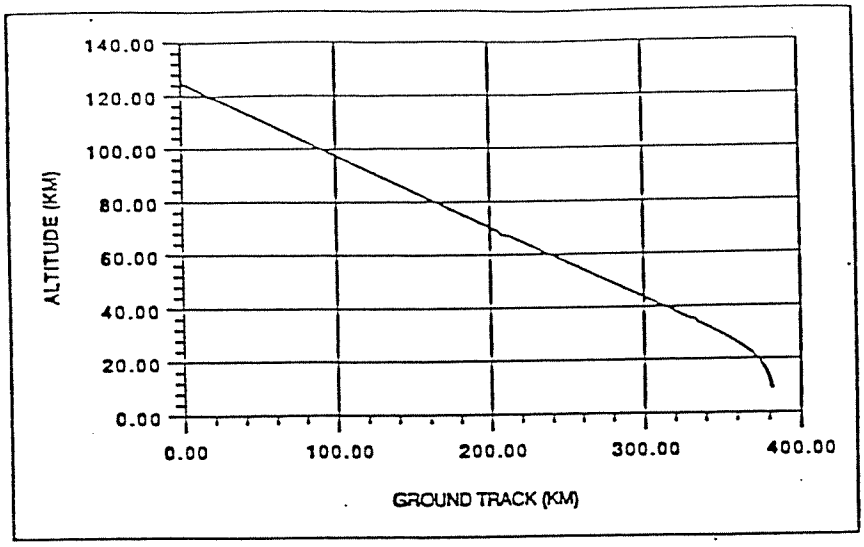

Figure 9. Mars Aerobrake Nominal Trajectory Ground Track History

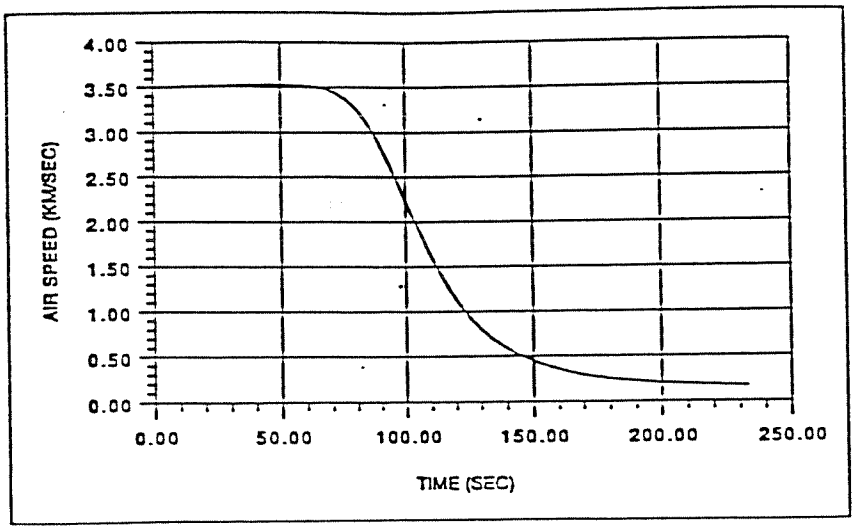

Figure 10. Mars Aerobrake Nominal Trajectory Velocity History

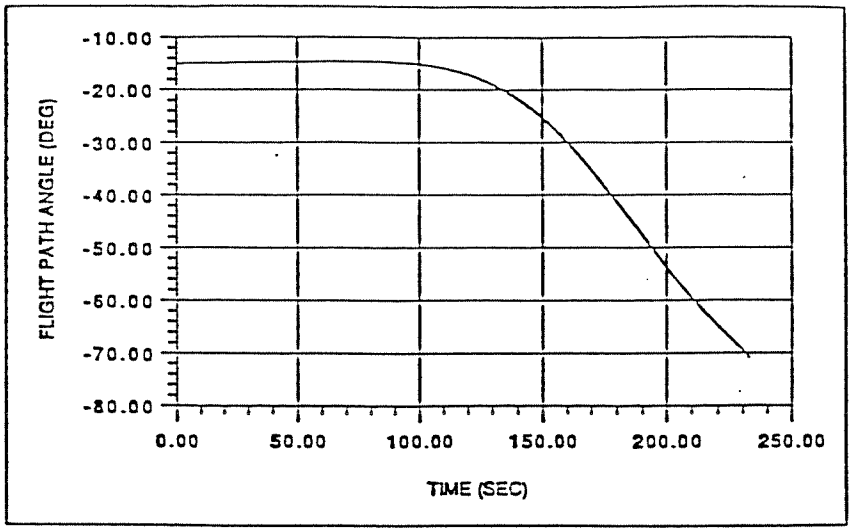

Figure 11. Mars Aerobrake Nominal Trajectory Flight Path History

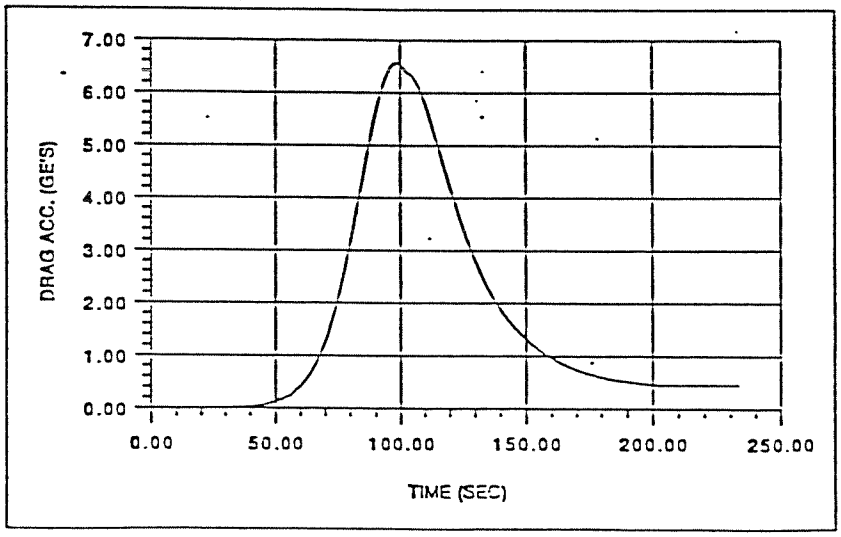

Figure 12. Mars Aerobrake Nominal Trajectory Drag History

Table 3. Aerobrake Entry-to-Landing Accuracy

B= 15/m2, VE = 3.5 km/s, I = 57.5 degrees, HE = 125 km, Gamma = -15 degrees

Input Error Source				Control (Act-Nom)		Knowledge (Act-Nav)	
Parameter	Description	Value (3 sigma)	Units	Downrange Miss (km)	Crossrange Miss (km)	Downrange Miss (km)	Crossrange Miss (km)
C/D	Drag Coefficient	5	%	1.618	-0.001		
Rho	Density Uncertainty	High		1.159	0.000		
	Daily	Low		0.638	0.001		
Gamma a	Entry Flight Path	0.015	degree	-0.362	0.000		
	Angle Control	-0.015	degree	0.363	0.000		
uw	Tail Wind	10	m/s	1.307	0.005		
	Head Wind	10	m/s	-1.309	-0.005		
vw	Cross Wing	10	m/s	-0.009	1.193		
Subtotal of RSS				2.838	1.193		
u	Knowledge of Entry	0.9	km			-0.867	0.051
	Position - Downtrack	-0.9	km			0.867	-0.052
V	Knowledge of Entry	0.9	km			-0.053	-0.873
	Position - Crosstrack	-0.9	km			0.052	0.873
W	Knowledge of Entry	0.9	km			0.110	-0.014
	Position - Vertical	-0.9	km			0.110	-0.012
u	Knowledge of Entry	0.1	m/s			-0.023	0.001
	Position - Downtrack	-0.1	m/s			0.023	-0.002
v	Knowledge of Entry	0.1	m/s			0.000	-0.029
	Position - Crosstrack	-0.1	m/s			0.001	0.023
w	Knowledge of Entry	0.1	m/s			0.003	0.000
	Velocity - Vertical	-0.1	m/s			-0.007	0.000
Subtotal of RSS						1.239	1.237
EV	Initial Gyro Misalign	82	arc sec			0.000	0.000
GCDR	Gyro Drift	0.023	deg/hr			0.000	0.000
B	Accelerometer Bias	17	ug			0.000	0.000
SF	Acccelerometer Scale	70	ppm			0.030	0.000
ALMT	Accelerometer Misalign	82	arc sec			0.000	0.000
Subtotal of RSS						0.030	0.000
TOTAL RSS				2.838	1.193	1.239	1.237

AEROMANEUVER ANALYSIS

The aeromaneuvering option was baselined in previous MRSR studies since it provided the capability to aerodynamically maneuver precisely to a prescribed target altitude over a landing site. It would allow the entry vehicle a long flight trajectory to make observations, process the observations and update its navigated state. The aeromaneuvering option has the added advantage of having a large maneuver footprint to access landing sites. Aeromaneuvering would reuse the aerocapture aeroshell.

The baseline aerodynamic configuration for the aero-maneuvering entry-to-landing segment of the MRSR mission assumes reuse of a portion of the aerocapture aeroshell. For aerocapture, the entry vehicle was flown at maximum L/D to minimize the effects of large projected navigation uncertainties. For aeromaneuvering, the ballistic coefficient, $B = m/C_D A$, needs to be minimized to effect minimum velocity at altitude over a target area for parachute deployment. This requires the entry vehicle to fly at C_{Lmax} where C_D is also maximized. For the baseline design, where the entry mass design goal is not to exceed 2640 kg for either the sample return lander or rover lander, this results in the following entry characteristics:

$$C_{Lmax} = 0.5 \text{ and } C_D = 0.91$$

$$B = 183 \text{ kg/m}^2,\ D = 4.5 \text{ m},\ L/D = 0.55,\ \alpha = 40° \text{(angle of attack)}$$

Entry Corridor

The entry corridor was calculated assuming deorbit and entry from a 500 km x 1500 km orbit. This results in an entry speed of about 3.5 km/s at an altitude of 125 km. Table 4 shows the results of trajectories where full lift-up is employed in a high density atmosphere. This will be used to define the overshoot boundary. Table 5 shows the results of trajectories where full lift-down is employed in a low density atmosphere. This will be used to define the undershoot boundary. Assuming that the shallowest entry would not result in a ballistic lob, the overshoot boundary can be expected to be between -3.5 and -4.0 degrees. To verify this, unbiased closed-loop guided trajectories were flown into a nominal range of about 2333 km as shown in Tables 6 and 7. The multiple values at a given flight path angle represent results at the mean, high and low COSPAR atmosphere models. This would suggest that -3.75

Table 4. Overshoot Boundary for L/D = 0.55

Gamma E (degrees)	Lat (degrees)	Long (degrees)	VI (km/sec)	Gamma I (degrees)	RG (degrees)	Mach No.	D max (ge's)	q max (knt/m2)	Q max (w/cm2)	Q total (kj/cm2)	TF (seconds)
-3.5	infinity					1.5	0.6	0.9	3.0	2.4	1697.3
-4.0	57.262	-78.832	0.4	-23.9	73.485	1.5	0.6	0.9	4.0	2.2	1450.2
-4.5	55.119	-103.002	0.4	-23.7	59.877	1.5	0.6	1.0	5.0	2.0	1299.6
-5.0	51.605	-115.384	0.4	-23.4	51.673	1.5	0.7	1.1	5.0	1.8	1192.2
-5.5	48.376	-122.820	0.4	-23.3	45.885	1.5	0.8	1.3	6.0	1.7	1109.4
-6.0	45.584	-127.827	0.4	-23.6	41.462	1.5	1.0	1.6	6.0	1.6	1042.5
-6.5	43.176	-131.467	0.4	-24.0	37.911	1.5					

Table 5. Undershoot Boundary for L/D = 0.5

Gamma E (degrees)	Lat (degrees)	Long (degrees)	VI (km/sec)	Gamma I (degrees)	RG (degrees)	Mach No.	D max (ge's)	q max (knt/m2)	Q max (w/cm2)	Q total (kj/cm2)	TF (seconds)
-3.0	infinity					6.6	6.2	9.7	7.0	1.2	684.0
-3.5	43.7	-131.1	1.5	-31.7	38.5	6.8	6.5	10.2	8.0	1.0	524.8
-4.0	37.0	-139.2	1.5	-31.6	29.4	6.9	6.7	10.5	8.0	1.0	440.4
-4.5	33.3	-142.8	1.6	-31.6	24.6	7.0	6.9	10.9	9.0	0.9	385.2
-5.0	30.8	-145.0	1.6	-31.6	21.5	7.1	7.1	11.2	9.0	0.8	344.6
-5.5	28.9	-146.5	1.6	-31.6	19.2	7.2	7.4	11.6	9.0	0.8	313.1
-6.0	27.4	-147.7	1.6	-31.6	17.4						

Table 6. Unbiased Closed-Loop Guided Trajectories at 10-km Target Altitude

Entry Corridor Calculations: Entry and Landing

L/D = 0.55; Beta = 183 kg/m2; Phi = Guided degrees; Rho = MRL; VG = 3.5 km/sec; AzE = 30 degrees, Target Altitude = 10 kilometers

Gamma E (degrees)	Lat (degrees)	Long (degrees)	VI (km/sec)	Gamma I (degrees)	RG (degrees)	Mach No.	D max (ge's)	q max (knt/m2)	Q max (w/cm2)	Q total (kj/cm2)	TF (seconds)	Miss (kilometers) Downrange	Crossrnge
-3.75	44.762	-130.754	0.670	-24.0	39.409	2.93	1.0	1.58	6	1.5	837	9.0E-01	2.4
-3.75	44.778	-130.726	0.660	-24.1	39.434	2.83	0.9	1.40	5	1.6	874	2.4E+00	2.2
-3.75	44.646	-130.734	0.722	-21.9	39.335	3.30	1.1	1.76	6	1.4	803	-3.5E+00	-2.9
-4.00	44.724	-130.678	0.667	-24.6	39.418	2.90	0.9	1.37	6	1.5	882	1.4E+00	-1.5
-4.00	44.724	-130.695	0.676	-24.1	39.410	2.90	0.9	1.38	6	1.6	916	9.0E-01	-0.9
-4.00	44.783	-130.731	0.651	-20.7	39.435	2.90	0.9	1.42	6	1.5	860	2.5E+00	2.6
-4.25	44.723	-130.708	0.677	-21.1	39.403	3.00	1.0	1.58	6	1.5	930	6.0E-01	-0.6
-4.25	44.624	-130.434	0.422	-28.4	39.469	1.80	1.0	1.57	6	1.6	1008	4.4E+00	-13.0
-4.25	44.769	-130.726	0.663	-21.4	39.428	3.10	1.0	1.60	6	1.5	909	2.0E+00	1.9

Table 7. Unbiased Closed-Loop Guided Trajectories at 6-km Target

Gamma E (degrees)	Lat (degrees)	Long (degrees)	VI (km/sec)	Gamma I (degrees)	RG (degrees)	Mach No.	D max (ge's)	q max (knt/m2)	Q max (w/cm2)	Q total (kj/cm2)	TF (seconds)	Miss (kilometers) Downrange	Crossrnge
-4.00	45.302	-130.028	0.6	-33.9	40.156	2.6	1.0	1.6	5	1.6	873.0	-0.6	1.0
-4.00	45.372	-129.932	0.5	-33.0	40.253	2.1	0.9	1.5	5	1.6	918.7	-5.1	1.0
-4.00	45.237	-129.978	0.6	-27.8	40.134	2.7	1.0	1.6	6	1.5	845.3	-1.9	-3.2
-4.25	45.317	-129.856	0.5	-20.4	40.252	2.3	0.8	1.2	5	1.6	929.0	5.0	-3.5
-4.25	45.391	-129.843	0.5	-30.3	40.311	2.1	0.8	1.3	5	1.6	964.9	8.5	-0.9
-4.25	45.307	-129.991	0.6	-32.7	40.177	2.5	0.9	1.4	5	1.6	903.4	0.6	0.1
-4.50	45.384	-129.256	0.4	-20.4	40.597	1.7	0.9	1.4	6	1.6	1028.0	25.5	-18.6
-4.50	45.276	-130.017	0.4	-35.3	40.142	1.6	0.9	1.4	6	1.6	1041.0	-1.4	-0.4
-4.50	45.357	-129.952	0.5	-29.9	40.235	2.4	0.9	1.4	6	1.4	960.6	4.1	1.2

degrees could be used as the shallowest entry flight path angle. The nominal entry flight path angle will be dictated by an offset entry flight angle margin (i.e., -0.25 degree) and the navigation flight path angle uncertainties.

The projected entry flight path angle control uncertainties are small. The uncertainties are on the order of ±0.03 degree. This then suggests that -4.0 degrees would be nominal entry flight path angle. Tables 8 and 9 show the basis for the ±0.03 degree uncertainty.

Table 8. Deorbit Parameters

$\frac{D\gamma}{Dr_p} = 0.033$ degree/km	Entry flight path angle sensitivity to periapsis altitude control
$\frac{D\gamma}{D\Delta V} = -0.145 \frac{\text{degree}}{\text{m/s}}$	Entry flight path angle sensitivity to deorbit ΔV control
$\Delta V = 90$ m/	Deorbit ΔV from 500 x 1500 km orbit
$\gamma = -4.0$ degree	Entry flight path angle at 125 km altitude
$r_p = 3460$ km	Vacuum periapsis altitude after deorbit
$\Delta r_p = 0.9$ km	3σ orbit determination error
B = 17 mg	3σ accelerometer bias
SF = 70 ppm	3σ accelerometer scale factor
GCDR = 0.023 degree/hour	3σ gyro drift

Table 9. Expected Entry Flight Path Angle Control

Error Source	Error Output (Gamma-Degree)
Orbit Determination	2.97×10^{-2}
Accelerometer Bias	2.958×10^{-5}
Accelerometer Scale Factor	9.135×10^{-4}
RSS	0.03

Maneuver Footprint

The maneuver footprints were calculated which represent the locus of accessible targets given the aeromaneuvering capability of the entry vehicle at prescribed entry conditions.

Early in this study, it was suggested that the projected entry flight path angle control error would be on the order of ±0.5 degree as opposed to ±0.03 degree. Therefore, the inclination of the de-orbit state was made as high as possible assuming the maximum plane change capability of the aerocapture vehicle. The deorbit state inclination was set at 57.5 degrees as opposed to 45 degrees if one were to target a latitude of 45 degrees. This was done to place the target in the middle of the minimum maneuver footprint such that entry dispersions never saturated the aeromaneuvering capability over the entry trajectory.

Figures 13 through 15 show the maneuver footprints for a nominal entry flight path angle of -4.0 degrees at an inclination of 57.5 degrees for three different de-orbit points and entry states along the 57.5-degree inclined orbit. The data demonstrate that latitudes of 57.5 degrees are accessible at the outer edge (cross ranging) of the maneuver footprint for a nominal entry state (-4.0 degrees). Figure 16 is a reprint of Figure 15 with a maneuver footprint superimposed with a flight path angle control error of -0.5 degree (-4.5 degree). It shows that over 50 percent of the accessible target area is lost including all targets at latitudes of 57.5 degrees. This is only for one dispersion. A target, though, at a latitude of 45 degrees (i.e. Alba Plains) can be readily centered. Entry flight path angle control errors of 0.03 degree will require less of an inclination offset ($\Delta i < 12.5$ degrees). The actual inclination offset was not quantified, since it was later discovered that the flight path angle control error would be

much less than ±0.5 degree. It does, though, demonstrate the importance of the entry interface delivery for maneuver footprint control.

CONTROL

The flight control during entry for aeromaneuvering would be mechanized in the same manner as for aerocapture which uses primarily a bank-to-turn steering technique. Bank-to-turn steering controls the lift vector orientation by controlling the vehicle bank angle. The vehicle is fixed trim, i.e. the angle of attack is passively stabilized to its nominal value of 40 degrees.

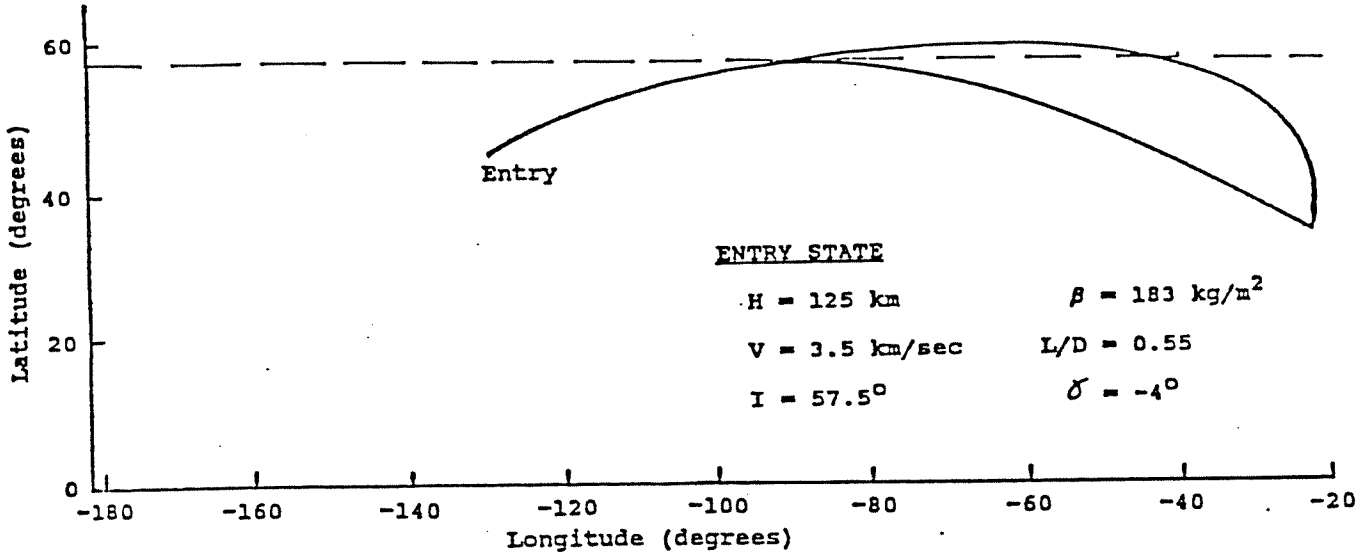

Figure 13. Entry Latitude 45°N Maneuver Footprint

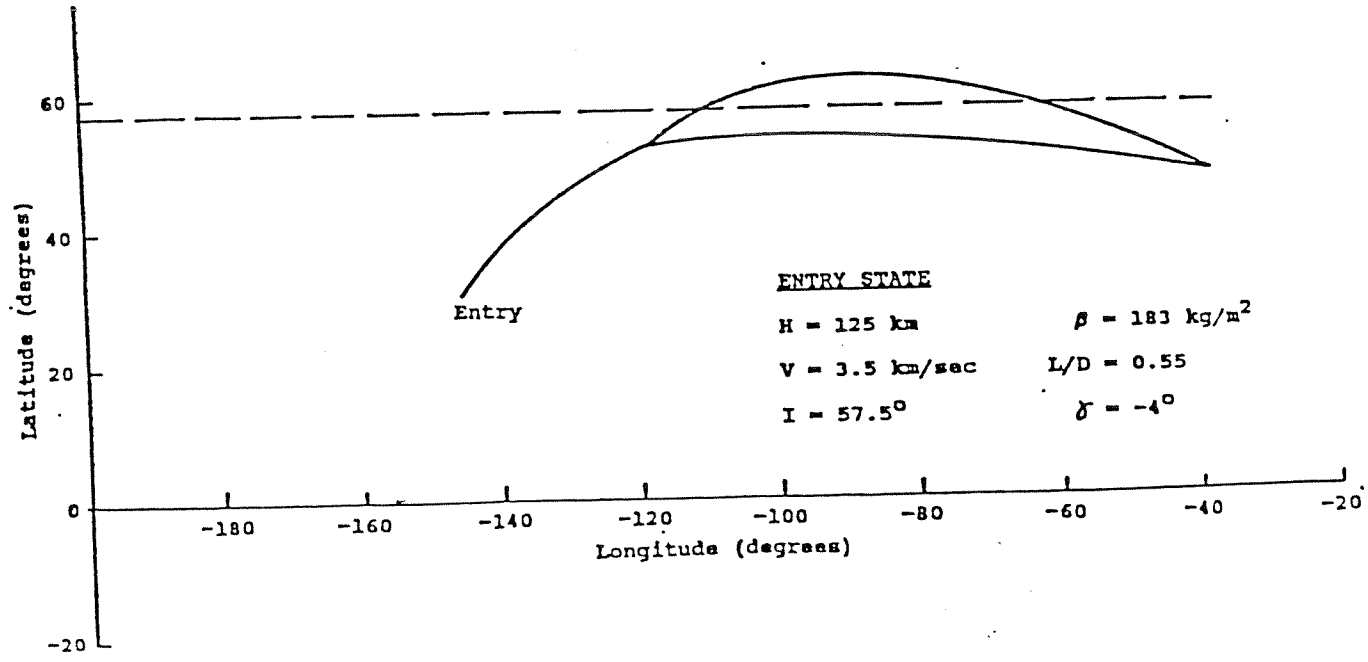

Figure 14. Entry Latitude 30°N Maneuver Footprint

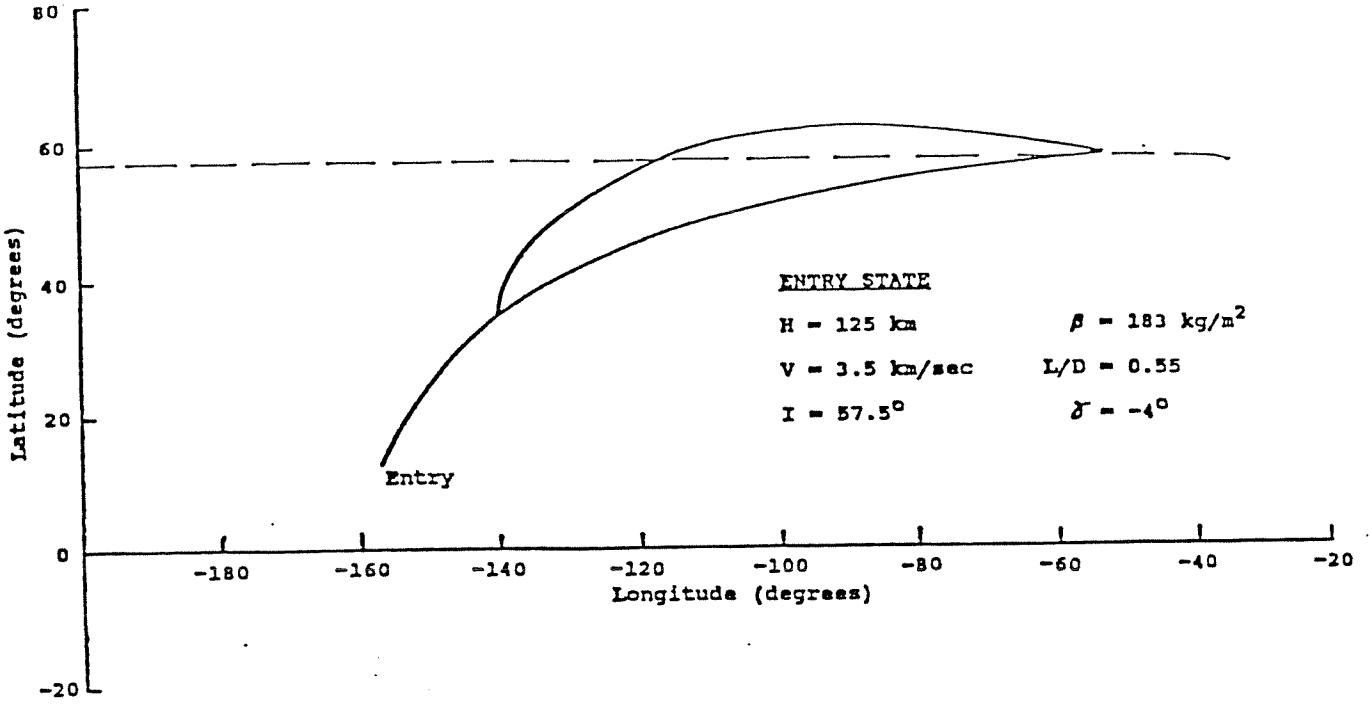

Figure 15. Entry Latitude 12.5°N Maneuver Footprint

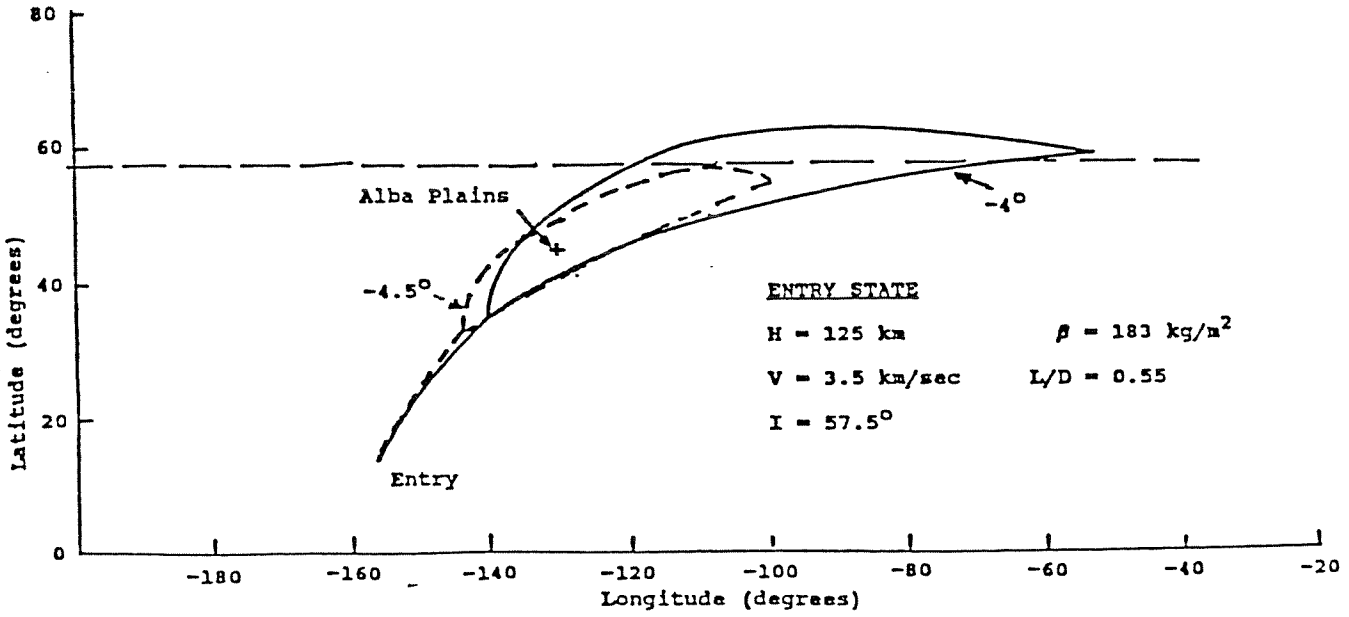

Figure 16. Entry Latitude 12.5°N Maneuver Footprint Reduction with -0.5° Delta-Gamma Error (-4.5°)

Guidance

In aeromaneuvering to a prescribed target site, the entry vehicle uses its constant angle of attack lift to fly an analytic reference trajectory by roll modulation. The basic guidance logic performs three primary functions: trajectory parameter prediction, targeting, and attitude command generation. The guidance first performs program sequencing and range predictions, and then the controller converts these data into attitude commands that are provided to the autopilot for execution. An analytic reference trajectory is recomputed each computer cycle (one second) to correct for range errors.

On the basis of this recomputed reference trajectory, a reference L/D, drag level, and rate of climb are analytically computed and provided to the controller. The controller (Equation 1) uses the L/D reference to maintain the proper flight profile, the difference between the measured drag(D) and drag reference(D_{ref}) term to control the range error, and the difference between the computed rate of climb($\dot{R}$) and the rate of climb reference($\dot{R}_{ref}$) to provide trajectory damping.

$$L/D = (L/D)_{ref} + C_1(D - D_{ref}) + C_2(\dot{R}_{ref} - \dot{R}) \qquad (1)$$

Here C_1 and C_2 are guidance gains chosen to optimize guidance law performance (see Reference 3).

The guidance logic is divided into four major phases and their duration may vary depending on the mission requirements as shown in Figure 17. These phases are pre-entry, constant drag, equilibrium glide and variable drag. A subphase which controls crossrange error is used in all the phases with the exception of pre-entry. This subphase issues bank-reverse-bank roll commands which keep the vehicle along a prescribed horizontal corridor (trapezoid of 30 km at entry to 1.0 kilometer at target for this paper) or track. The L/D controller is mechanized the same as in the reference aerocapture studies.

Pre-entry Phase

The purpose of the pre-entry phase is the computation of the attitude hold commands prior to atmospheric entry and the beginning of the computation of the entry targeting data. Prior to 0.05 g's, the entry vehicle is in a three-axis-attitude-hold mode. At 0.05 g's, vehicle rate damping is initiated and the guidance transfers to the constant drag phase.

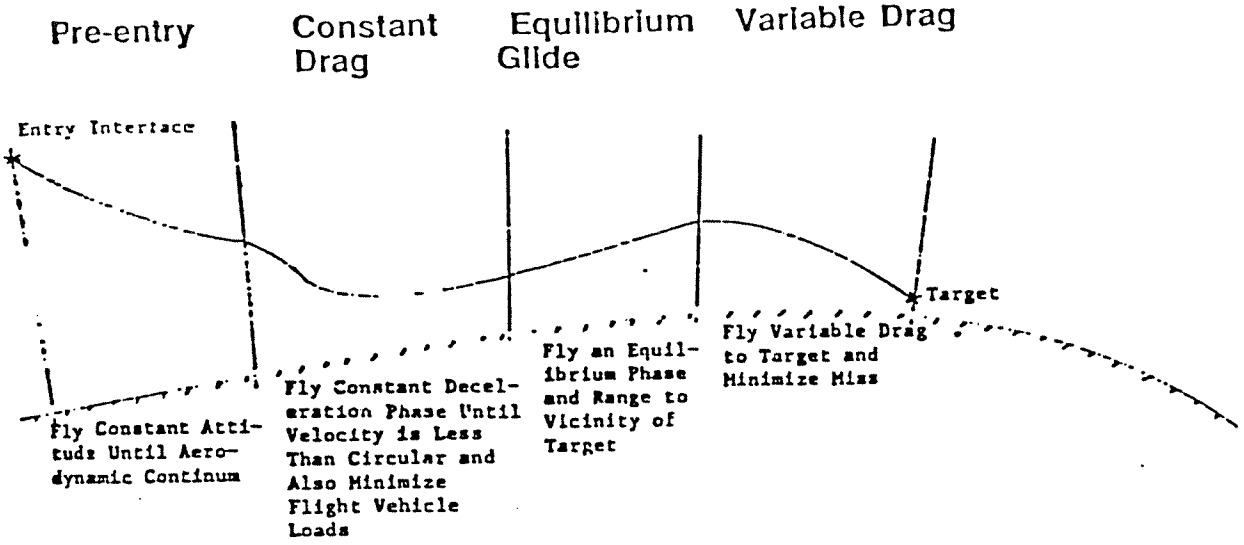

Figure 17. Entry to Landing Targeting

Constant Drag Phase

The purpose of the constant drag phase is to limit vehicle flight loads and insure atmospheric capture (no exit) of the entry vehicle. The entry vehicle flies in this mode until its velocity is less than circular. No Kepler or exit trajectories for the purpose of range extension were considered. The constant drag phase is the same as used in the aerocapture. The reference constant drag level is optimized on vehicle limit loads and entry-to-target ranges (about 1.0 g).

Equilibrium Glide Phase

The purpose of the equilibrium glide phase is to range the entry vehicle flight trajectory in the vicinity of the prescribed target based on constant attitude range (R_{EQ}) estimates and range-to-go (R_{TG}). This phase is terminated when the R_{EQ} predicts that the current constant attitude vehicle flight trajectory will reach or overfly the target ($R_{EQ} \geq R_{TG}$). This phase is mechanized by the following reference conditions.

$$D_{Ref} = \frac{G}{(L/D)_{current}}\left[1 - \frac{V^2}{V_s^2}\right] \tag{2}$$

where

$(L/D)_{current}$ = current vehicle vertical plane L/D

$$(L/D)_{Ref} = (L/D)_{current} - \frac{4GH_s}{V^2(L/D)_{current}} \tag{3}$$

$$\dot{R}_{Ref} = \frac{-2GH_S}{V(L/D)current} \tag{4}$$

$$R_{EQ} = \frac{V_s^2}{2G}(L/D)current \log_e \left[\frac{V_T^2 - V_s^2}{V^2 - V_s^2} \right] \tag{5}$$

where

V_T = estimate of vehicle speed at the target altitude (6-10 km in most cases). This is approximately equal to the vehicle terminal airspeed at that altitude.

H_S= density scale height

G = value of gravity at the planet surface

V_S= satellite circular orbital speed at the entry altitude

Variable Drag Phase

The purpose of the variable drag phase is to null downrange target errors. This phase uses segmented constant drag phases to null R_{TG}. This phase is mechanized by Equation (1) with the following reference conditions:

$$D_{Ref} = \frac{V^2 - V_T^2}{2R_{TG}} \tag{6}$$

$$(L/D)_{Ref} = \frac{G}{D_{Ref}} \left[1 - \frac{V^2}{V_s^2} \right] \tag{7}$$

$$\dot{R}_{Ref} = \frac{-2H_S D_{Ref}}{V} \tag{8}$$

Performance Sensitivity

Aeromaneuver entry sensitivity analyses were performed to understand the trajectory profile influence on the entry flight loads, parachute deployment conditions, parachute deployment strategies and landing accuracy.

Trajectory Profile

Currently, the TRW entry to landing vehicle designs for the Mars Ascent Vehicle (MAV) segment of the MRSR mission have a mass of approximately 2640 kg. Assuming that the entry vehicle flies at $C_{L_{max}}$, this corresponds to a B of 183 kg/m^2 at an L/D of 0.55 with C_D of 0.91 and aeroshell base radius r_B of 2.25 meters. These aerodynamic characteristics are for hypersonic continuum atmospheric flight. The corresponding B for a rover segment could range from 183 kg/m^2 to 385 kg/m^2. The high range assumes that the rover entry and landing systems would grow to capitalize on the maximum throw weight of 7000 kg to Mars on a Titan Centaur. Also, the reason for flying the entry vehicle during the entry to landing segment at $C_{L_{max}}$ as opposed to L/D_{max} is that at L/D_{max}, B roughly triples in magnitude because the drag coefficient is reduced by a third. This increase in B would cause a large increase in required thermal protection mass. B of this magnitude would also significantly impact the parachute and terminal segments of the mission as we will see later.

In simulations, the entry vehicle normally flew to the target altitude required at the prescribed target latitude and longitude in an equilibrium glide. Normally, the minimum achievable parachute deployment speed is the terminal speed for an L/D < 1.0. This though is very difficult to achieve. The next best situation is where the lift is saturated in a pull out maneuver. This is an equilibrium glide at full lift. The speed at altitude would then be the terminal speed at altitude divided by the square root of the L/D. For an L/D = 0.55, this is the terminal speed times 1.35. These speeds correspond to Mach Number of about 2.3 and 2.97 at altitudes of 6 and 10 km, respectively, in the lowest density atmosphere. As the entry mass grows, it should be expected that parachute deployment Mach number and corresponding dynamic pressure will increase.

The results shown in Tables 6 and 7 correspond to different target altitudes. These were 10 and 6 km, respectively. The thing to note is the parachute deployment Mach Number which is closing in on a Mach 3 parachute deployment requirement; another thing to note is the reduction in the aerodynamic peak loads and the convective heating rates as compared to aerocapture (3 g's and 160 w/cm^2). The aerodynamic peak load does not exceed 1.0 g. The heating rates are also about two orders of magnitude lower. Figures 18 through 23 show the detailed time histories of the nominal aeromaneuver trajectory.

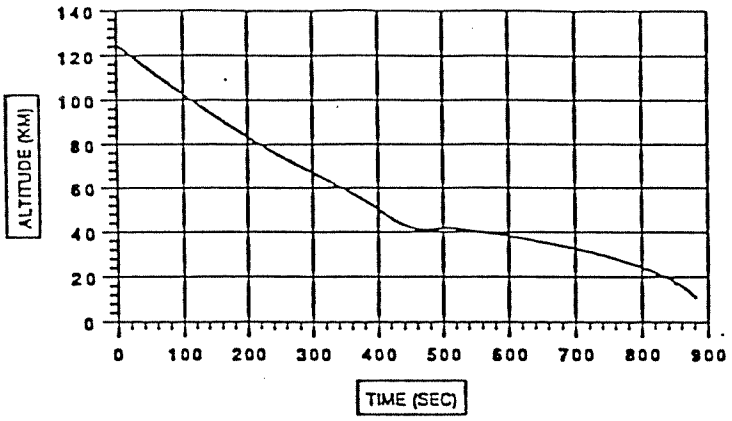

Figure 18. Mars Aeromaneuvering Nominal Trajectory Altitude History

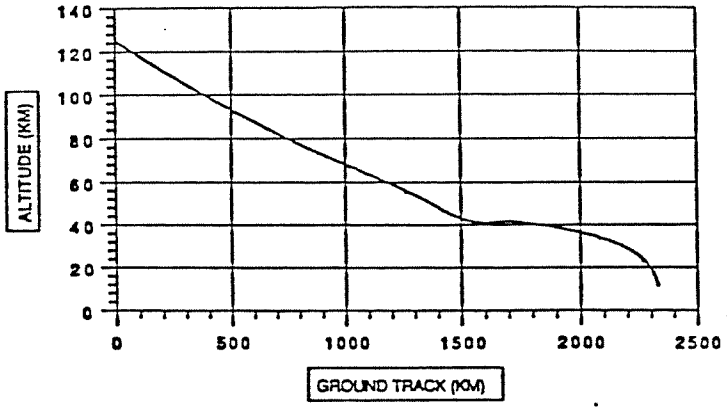

Figure 19. Mars Aeromaneuvering Nominal Trajectory Ground Trace History

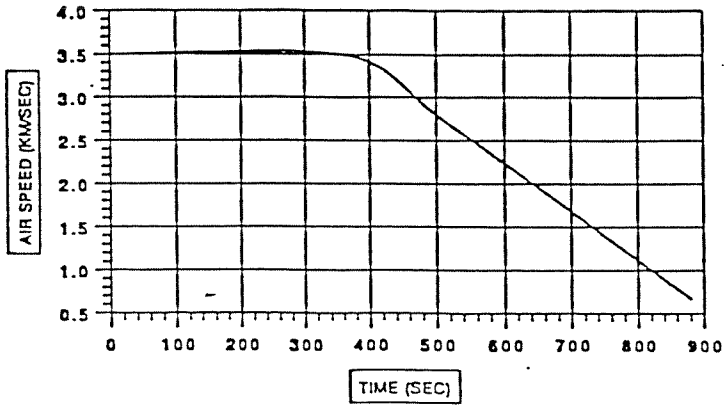

Figure 20. Mars Aeromaneuvering Nominal Trajectory Velocity History

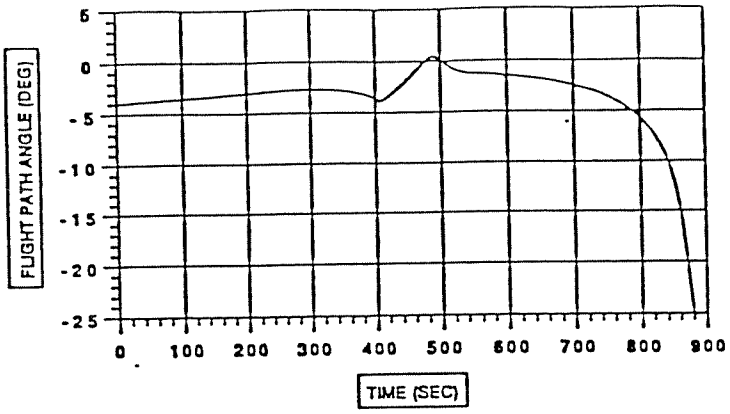

Figure 21. Mars Aeromaneuvering Nominal Trajectory Flight Path Angle History

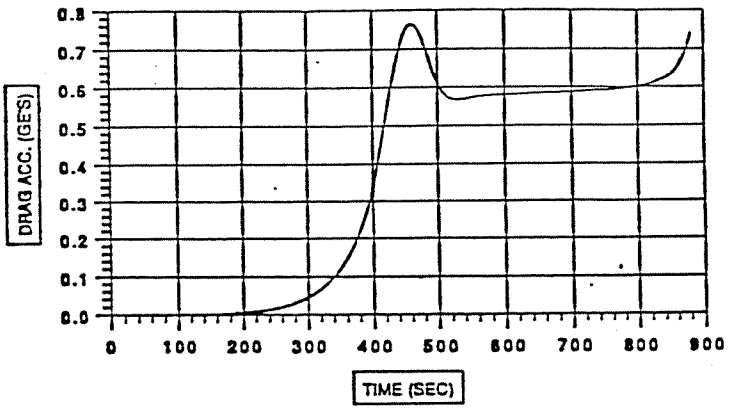

Figure 22. Mars Aeromaneuvering Nominal Trajectory Drag History

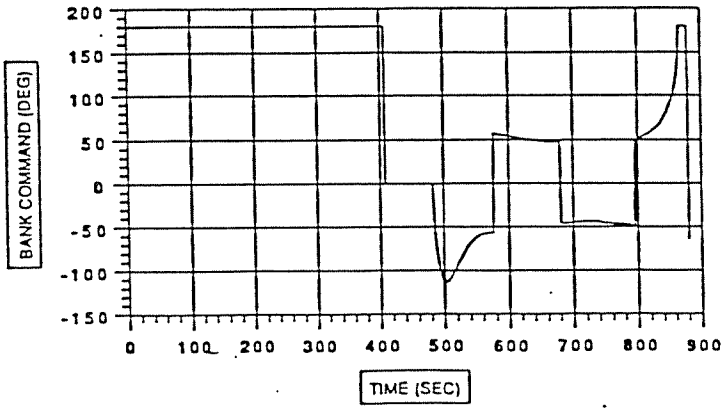

Figure 23. Mars Aeromaneuvering Nominal Trajectory Bank Command History History

Parachute Deployment Conditions

Using the current scenario for terminal descent where a parachute is deployed at altitude followed by a propulsive soft landing, a number of constraints must be met. These are as follows:

1. The parachute deployment Mach number and dynamic pressure must be constrained to meet parachute design limitations in terms of heating, material loads and reefing/canopy inflation. The current state of the art is about a maximum of Mach 2.1 and 1000 N/m^2 dynamic pressure. Otherwise, a potentially significant parachute technology development may be required (i.e., Mach 3 and 2250 N/m^2).

2. The parachute deployment altitude must be constrained to allow sufficient time for parachute terminal descent to damp out lander nutation, to acquire and track landmarks and to be near terminal descent (falling vertically) for propulsive lateral translation and soft landing. Optimally, this corresponds to about a 10 kilometer altitude for a target at the aeroid and to about a 12 km altitude relative to the aeroid for a target at about 2.5 km above the aeroid.

Figure 24 shows the minimum Mach number achievable at a given altitude above the aeroid for the COSPAR low atmosphere (Reference 1) and a range of entry B prior to parachute deployment. The minimum Mach number assumes that the entry vehicle is in a terminal descent at parachute deployment. Achieving this minimum will require judicious entry trajectory shaping. The Mach 2 and 10 kilometer altitude point corresponds to the desired conditions which would allow about 73 seconds on the parachute and a flight path angle of about -80 degrees before the propulsive segment of the descent phase of the mission. This suggests that the entry B should be

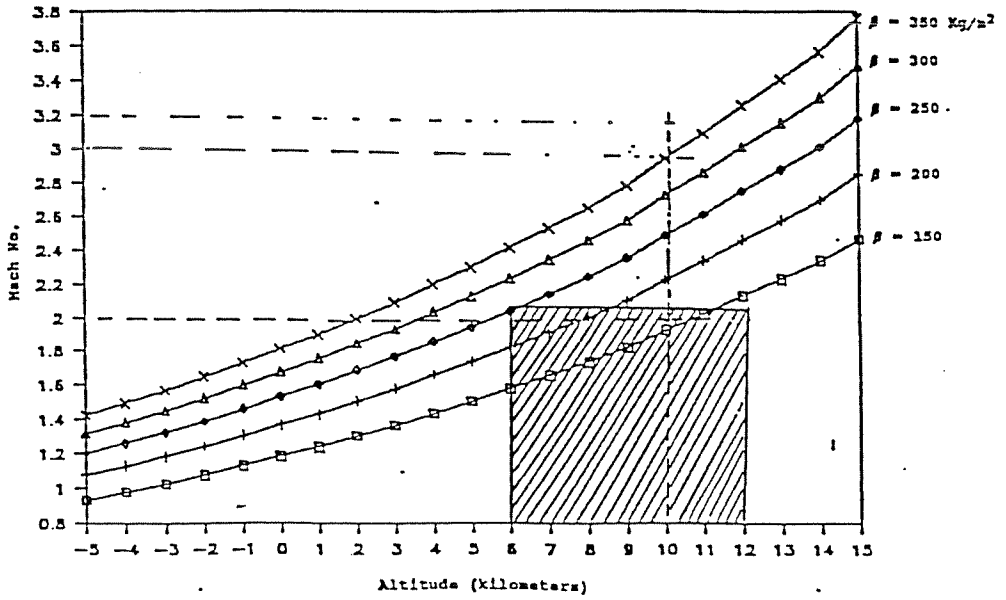

Figure 24. Effect of Beta on Mach Number at Altitude

constrained to about 160 kg/m^2 or less. For targets of about 2.5 kilometer altitude, the B should be constrained to about a maximum of about 140 kg/m^2. If the time required on the parachute could be decreased to 38 seconds and a flight path angle of about -62 degrees before the propulsive segment, the parachute deployment altitude could be reduced to 6 km which would also constrain targets to the aeroid. This would allow B to be as high as 240 kg/m^2. For the lowest B in our designs of 183 kg/m^2 the parachute deployment altitude would probably have to be lowered to about 8 km which allows about 60 seconds on the parachute. Constraining the entry weight not to exceed 2640 kg regardless of the payload would allow use of current parachute designs.

Allowing the Mach number to be as high as required (i.e., Mach 3.2 and 2250 N/m^2) would allow the 385 kg/m^2 B entry vehicle. In addition, this would help the landing accuracy by releasing a constraint in the entry to landing guidance process. The entry vehicle can then be allowed to steer closer to the target regardless of altitude and parachute deployment Mach number and dynamic pressure constraints.

The effect of winds on this parachute deployment was also investigated, since this is potentially one of the driving contributors to the landing accuracy estimates. In addition, the effect of the parachute deployment altitude was investigated assuming that the entry vehicle would arrive at the same flight path conditions at various altitudes and deploy a parachute. This implies that the entry vehicle would have the B required to reach these conditions. The parachute was sized such that the terminal speed at 2 kilometer altitude would be about 100 m/s (B = 15 kg/m^2).

Table 9 summarizes the effects of winds when the parachute is deployed at an altitude of 6 km and at about Mach 2.25 which corresponds to the upper range where a 183 kg/m^2 B entry vehicle might operate. This table considered winds of 5 to 40 m/s acting either as a tail, cross or head wind. The misses associated with each component are of the same magnitude with the tail winds imparting slightly higher misses. These misses range from 0.15 km to 1.3 km. The table also shows the magnitude of the deceleration loads in g's and dynamic pressure when the parachute is assumed to instantaneously deploy. Depending on how the parachute is reefed and the canopy inflated, these loads could be different. This table, though, suggests potential loads as high as 10 g's. Tables 10 and 11 present the results for parachute deployment at altitudes of 10 and 15 km, respectively. The target misses double at 10 km and triple at 15 km when compared to parachute deployment at 6 kilometer altitude. The instantaneous parachute deployment loads are a factor of two less at 15 kilometer altitude.

The time of descent (TF) to 2 km altitude is best at 15 km with about 105 seconds of free fall. The requirement for time of descent has yet to be determined. This requirement is driven by the time required to reorient the lander as it exits the aeroshell, to damp nutation, to acquire and track landmarks, and to reach terminal descent conditions for the propulsive phase.

Table 9. Effect of Parachute Deployment at 6-Kilometer Altitude

Wind		Gamma	V	T_F	Miss - km			D_{max}	q_{max}
Magnitude (m/sec)	Direction	(deg)	(m/sec)	(sec)	Downrange	Crossrange	RSS	(g's)	(knt/m^2)
40	Tail	-62.3	98.5	39.2	0.911	-0.875	1.263	9.4	1.39
40	Cross	-62.4	99.2	38.3	-0.743	-0.782	1.079	8.3	1.22
40	Head	-62.6	99.9	37.2	-0.840	0.806	1.164	7.1	1.06
20	Tail	-62.3	98.8	38.7	0.447	-0.429	0.620	8.8	1.30
20	Cross	-62.4	99.2	38.3	-0.372	-0.389	0.538	8.3	1.22
20	Head	-62.4	99.5	37.7	-0.429	0.412	0.595	7.7	1.13
10	Tail	-62.3	99.0	38.5	0.221	-0.213	0.307	8.5	1.26
10	Cross	-62.4	99.2	38.3	-0.186	-0.194	0.296	8.3	1.21
10	Head	-62.4	99.3	38.0	-0.217	-0.208	0.301	8.0	1.17
5	Tail	-62.3	99.1	8.4	-0.110	-0.106	0.153	8.4	1.24
5	Cross	-62.4	99.2	38.3	-0.093	-0.097	0.134	8.3	1.21
5	Head	-62.4	99.3	38.1	-0.109	0.104	0.151	8.1	1.19

Table 10. Effect of Parachute Deployment at 10 Kilometer Altitude

Parachute Jettison at 2 Kilometers Altitude
Low Density Cospar Model
Conditions at Parachute Deployment: H = 10 km, V = 530.5 m/sec, Gamma = -25°, AZ = 44°

Wind		Gamma	V	T_F	Miss - km			D_{max}	q max
Magnitude (m/sec)	Direction	(deg)	(m/sec)	(sec)	Downrange	Crossrange	RSS	(g's)	(knt/m^2)
40	Tail	-79.5	98.8	73.1	1.814	-1.742	2.515	6.6	0.97
20	Tail	-79.5	98.8	72.6	1.814	-0.861	1.243	6.2	0.91
10	Tail	-79.6	98.8	72.3	0.446	-0.428	0.618	6.0	0.88
5	Tail	-79.6	98.8	72.1	-0.222	-0.213	0.308	5.9	0.86

Table 11. Effect of Parachute Deployment at 15 Kilometer Altitude

Parachute Jettison at 2 Kilometers Altitude
Low Density Cospar Model
Conditions at Parachute Deployment: H = 15 km, V = 530.5 m/sec, Gamma = -25°, AZ = 44°

Wind		Gamma	V	T_F	Miss - km			D_{max}	q max
Magnitude (m/sec)	Direction	(deg)	(m/sec)	(sec)	Downrange	Crossrange	RSS	(g's)	(knt/m^2)
40	Tail	-85	100.4	106.2	2.645	-2.540	3.667	4.1	0.61
20	Tail	-85	100.3	105.6	1.311	-1.259	1.818	3.9	0.57
10	Tail	-85	100.3	105.2	0.653	-0.627	0.905	3.8	0.55
5	Tail	-85	100.3	105.2	0.325	0.312	0.451	3.7	0.54

Parachute Deployment Strategies

Two feasible parachute-assisted descent strategies were developed. The first strategy (hereafter referred to as Type I strategy) is used when the velocity of the vehicle is Mach 2 at 10 km altitude and the second (hereafter referred to as a Type II strategy) is used when the velocity is Mach 3. In both cases, all terminal condition requirements are met and suggested parachute sizes are given.

Figure 25 shows a schematic of the system during a typical Type I descent strategy. A Type II descent strategy would only entail Configurations A and B (see Figure 25) prior to release of the MAV just prior to the final landing phase of the mission.

The objective of the descent strategy is to get the vehicle down from the terminal conditions of the aeromaneuver (10 km altitude, Mach 2 or Mach 3) to the proper orientation, altitude, and speed prior to the final landing phase. The final landing phase requires the vehicle to be upright (legs pointing vertically down) with a velocity near 100 m/s at an altitude of 2 km (Configuration D in Figure 25).

The Type I descent sequence from Mach 2 is:

1. Deploy the aeroshell parachute out of the side of the aeroshell nose in order to reorient and slow the aeroshell/MAV combination.

2. When the aeroshell/MAV combination has been reoriented and the pitch rate is small, release the MAV from the aeroshell.

3. Deploy the MAV parachute from the nose of the MAV in order to slow the MAV down to 100 m/s.

4. Start propulsive descent when the MAV is down to 2 km altitude.

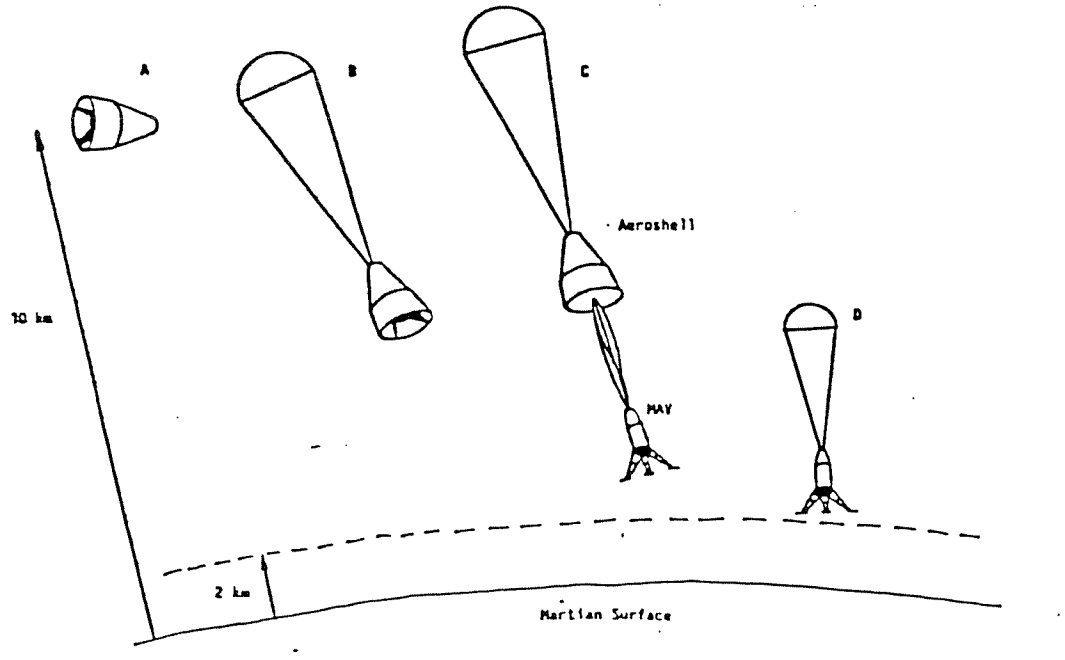

Figure 25. Schematic of MRSR Dynamic System

The Type II descent sequence from Mach 3 is:

1. Deploy the first parachute out of the side of the aeroshell nose in order to reorient and slow the aeroshell/MAV combination.

2. When the aeroshell/MAV combination is down to Mach 2, release the first parachute and deploy the second parachute.
3. Start propulsive descent when the aeroshell/MAV combination is down to 2 km altitude.

For the Type I strategy, the trajectories, pitch angle time histories, accelerations, and pitch angle rates shown in Figures 26 through 29 are obtained. Looking specifically at Figure 26, the first few seconds are spent turning the aeroshell/MAV around. During the next 40 seconds the resulting 60°/1.2 rad/sec oscillation is damped out prior to separation of the MAV from the aeroshell. The peak accelerations are about 4 g's axial and 5 g's lateral. Separation of the MAV from the aeroshell and deployment of the MAV parachute occurs at 48 seconds when the vehicle is aligned with the velocity vector within 6 degrees and the pitch rate is less than 0.2 rad/sec. Approximately one second later, the cables between the MAV and its parachute become taut and induce the accelerations and oscillations which can be seen in Figures 28 and 29. Following damping of this oscillation, the MAV/parachute combination drifts down to the final altitude of 2 km. At 2 km altitude, the MAV has travelled approximately 13 km downrange and has a velocity of 102 m/s.

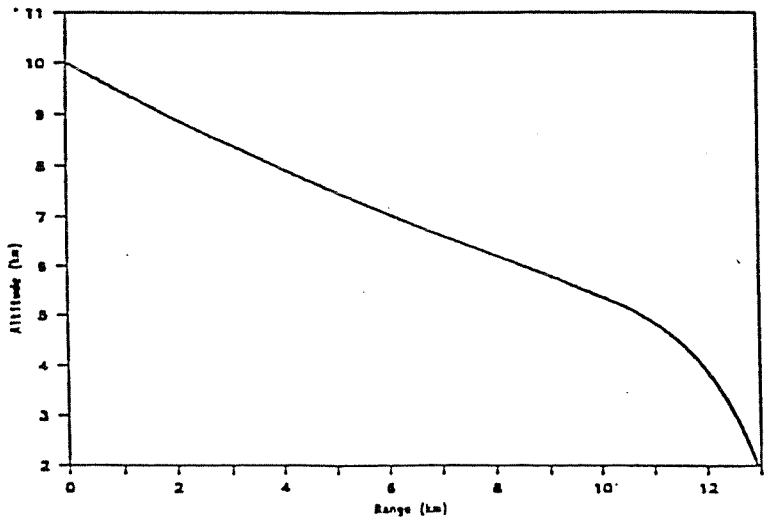

Figure 26. MAV Descent Trajectory, Type I Strategy

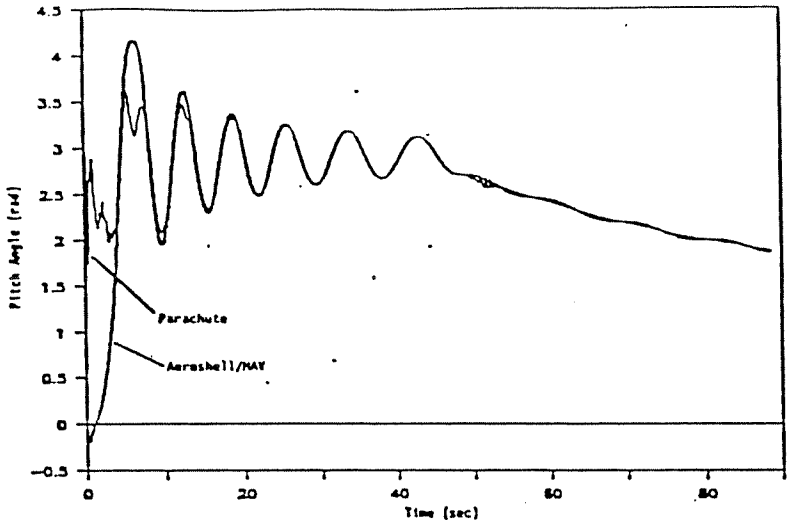

Figure 27. MAV and Parachute Pitch Angle Time Histories, Type I Strategy

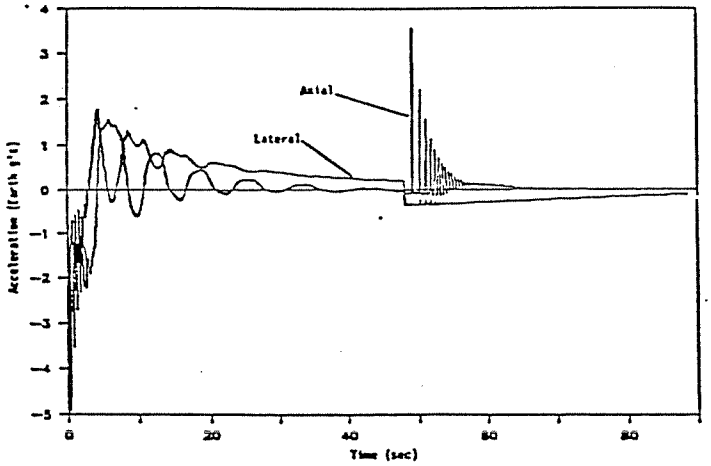

Figure 28. MAV Accelerations, Type I Strategy

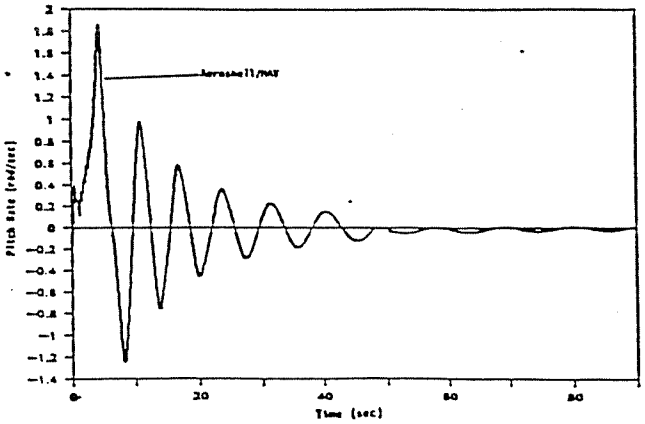

Figure 29. MAV and Parachute Pitch Angle Rate Time Histories, Type I Strategy

For Type II strategy, the trajectories, pitch angle time histories, accelerations, and pitch angle rates shown in Figures 30 through 33 are obtained. Again, the first few seconds are spent turning the aeroshell/MAV around. When the aeroshell/MAV combination has slowed to Mach 2 at approximately 8 seconds, the first parachute is released and the second is deployed. The accelerations from the deployment of the second parachute can be seen in Figure 32. The aeroshell/MAV combination continues down to the final altitude of 2 km. At 2-km altitude, the MAV has travelled approximately 19 km downrange and has a velocity of 76 m/s. In terms of accelerations and oscillations magnitude, strategy II is not much different than strategy I.

Both descent strategies have been found to be relatively insensitive to deployment timing regarding the terminal conditions. For the Type I strategy, the alignment tolerance of the MAV/aeroshell combination with its velocity vector and the MAV/aeroshell pitch rate prior to MAV/aeroshell separation can be varied to a large degree without significantly affecting the overall descent strategy (provided the MAV does not hang up on the aeroshell during separation). For the Type II strategy, the initial turnaround maneuver is somewhat sensitive to the size of the parachute and its guy wires regarding the tangling of the parachute guy wires, but the terminal conditions are insensitive to the second parachute deployment time.

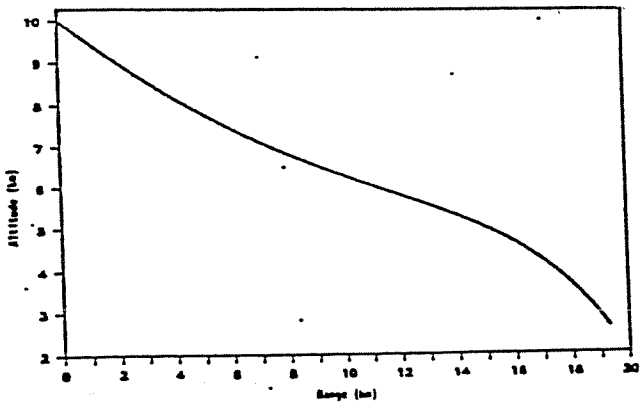

Figure 30. MAV Descent Trajectory, Type II Strategy

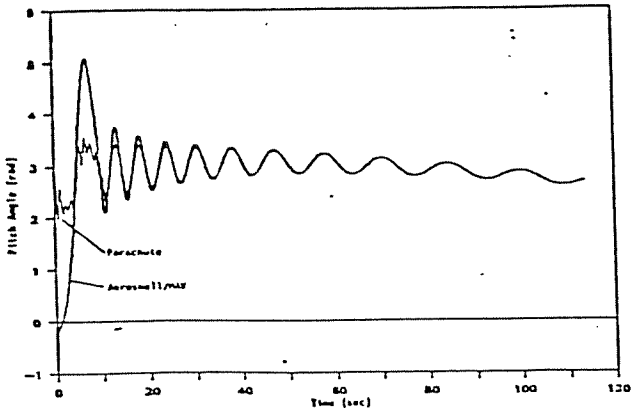

Figure 31. MAV and Parachute Pitch Angle Time Histories, Type II Strategy

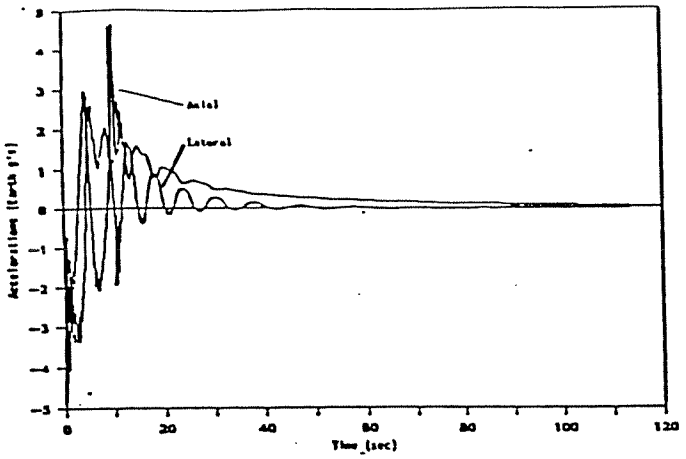

Figure 32. MAV Accelerations, Type II Strategy

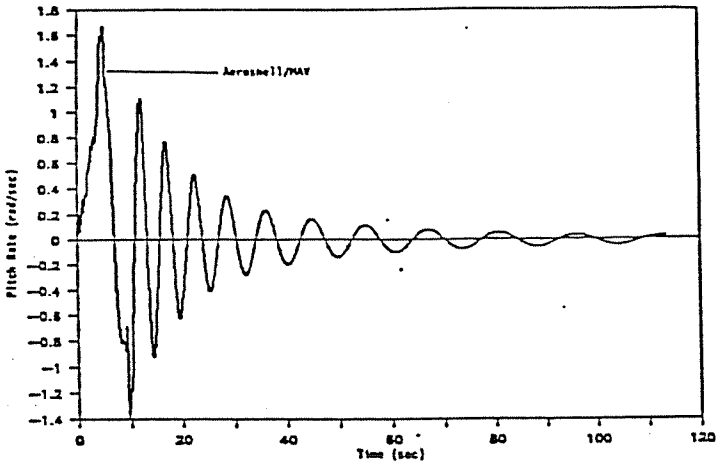

Figure 33. MAV and Parachute Pitch Angle Rate Time Histories, Type II Strategy

Landing Accuracy

For the aeromaneuvering entry-to-parachute deployment phase, three types of error contributors were analyzed to determine potential landing dispersions. These were dispersions to a nominal ideal guidance flight path control, initial knowledge of navigated state and sensor accumulated error. There were two components calculated which reflect deviation from nominal (ACT-NOM) and knowledge of the current from actual (ACT-NAV). These reflect the control and knowledge errors. The latter component does not apply to the ideal guidance errors. Table 12 shows a breakdown of these errors into three sets made up of a total of 22 individual perturbations. The cross range miss at the target altitude results from the bank-to-turn steering mechanization which relies on bank-reversals. The ideal guidance control error and the initial state knowledge errors are dominant. The IMU sensor error is comparatively small.

Summing all errors in an RSS sense including combined downrange and crossrange, a 6 kilometer propulsive ΔV capability would be required to effect pin point landing. This assumes that a terminal fix system helps the flight computer realize its position uncertainty in control and knowledge to pin point land. The major contributors in the analysis are the ideal guidance mechanization which results in about 2 to 3 km and the control error resulting from the navigation knowledge initialization errors. This is followed by the navigation knowledge initialization propagation. The IMU sensor accumulated knowledge and control error are the smallest contributors. The final terminal error or uncertainties are of equal magnitude. They are a result of mapping the aerographic landmarks to a suitable inertial coordinate system and the drift on the parachute due to winds.

Table 12. Aeromaneuvering Entry-to-Landing Accuracy Analysis for L/D = 0.55, b = 183 kg/m^2, VE = 3.5 km, I = 57.5 degrees, HE = 125 km, Gamma = -4.0

Input Error Source				Control (Act-Nom)		Knowledge (Act-Nav)	
Parameter	Description	Value (3 sigma)	Units	Down Range Miss (km)	Cross Range Miss (km)	Down Range Miss (km)	Cross Range Miss (km)
L/D	Lift to Drag Ratio Uncertainty	15	%	1.092	-1.326		
	Density Uncertainty	High		1.091	-1.709		
		Low		1.795	2.534		
Gamma a	Entry Flight Path Angle Control	0.03	degree	-0.077	0.219		
		-0.03	degree	0.616	0.594		
Subtotal of Root Sum Squared				2.447	3.391		
u	Knowledge of Entry Position - Downtrack	0.9	km	-0.487	0.033	-0.413	0.220
		-0.9	km	-0.244	-0.083	0.338	-0.013
V	Knowledge of Entry Position - Crosstrack	0.9	km	-0.279	-2.456	-0.076	-1.025
		-0.9	km	0.058	1.400	0.023	0.751
W	Knolwedge of Entry Position - Vertical	0.9	km	0.969	0.064	0.770	0.134
		-0.9	km	-0.719	0.625	-0.668	0.564
u	Knowledge of Entry Position - Downtrack	0.1	m/sec	-0.094	-0.121	-0.084	0.071
		-0.1	m/sec	0.064	-0.019	0.043	0.063
v	Knowledge of Entry Position - Crosstrack	0.1	m/sec	-0.112	-0.181	-0.031	0.003
		-0.1	m/sec	-0.093	0.279	-0.031	0.283
w	Knowledge of Entry Velocity - Vertical	0.1	m/sec	-0.016	-0.252	0.023	-0.129
		-0.1	m/sec	-0.121	0.005	-0.074	0.071
Subtotal of Root Sum Squared				1.372	2.930	1.161	1.453
EV	Initial Gyro Misalign	82	arcsec	-0.127	-0.117	-0.038	0.007
GCDR	Gyro Drift	0.023	deg/hr	-0.061	-0.381	-0.019	-0.257
B	Accelerometer Bias	17	ug	-0.201	-0.182	-0.092	-0.215
SF	Acccelerometer Scale	70	ppm	0.355	0.237	0.111	0.045
ALMT	Accelerometer Misalign	82	arcsec	-0.173	-0.420	-0.163	-0.228
Subtotal of Root Sum Squared				0.465	0.652	0.222	0.408
TOTAL ROOT SUM SQUARED				2.844	4.529	1.182	1.509

MARS TERMINAL DESCENT PHASE

Analysis

The aeromaneuver and aerobrake phases end when the lander reaches a specified altitude above the planet surface, 6 km for the aeromaneuver option and approximately 10 km for the aerobrake option. At this point, the Mars landing (or terminal descent) phase begins. The objectives of this phase are to 1) identify safe landing sites within a specified range and 2) bring the lander to a safe landing at the identified landing site. The terminal descent targeting function satisfies the first of these objectives, while the terminal descent guidance function satisfies the second objective. This section presents a description of the terminal descent guidance strategy and a brief description of its integration with the terminal descent targeting function.

One important issue in the design of the terminal descent guidance function is the development of a guidance law capable of determining the engine thrust required at each instant of time along the descent trajectory to guide the lander to a safe landing. Ideally, the lander should reach zero vertical velocity as it reaches the planet surface. The guidance law should also minimize the fuel required to safely reach the landing site. The guidance law must be robust in that it must work properly in the presence of navigated state uncertainties and unexpected disturbances (winds, atmospheric density shears, etc.) acting on the vehicle along the descent trajectory. The guidance law must also be in closed-loop form, i.e., thrust commands must be expressed as an explicit function of the lander's current position and velocity with respect to the specified landing site.

The Robust E-Guidance algorithm presented in this paper allows all of these requirements to be satisfied. This explicit closed loop algorithm calculates at each guidance interval the optimal thrust history required to achieve a soft landing at the desired site. Its robustness properties are further improved by the explicit inclusion of the effects of possible causes of trajectory dispersions in a worst case sense. The algorithm optimizes the performance of the terminal descent guidance function in the presence of these uncertainties and disturbances, thus keeping fuel consumption low while effecting a safe landing.

Targeting

Two landing options have been chosen for analysis: hazard avoidance and pinpoint landing. For hazard avoidance, the lander autonomously selects a safe landing site by identifying surface hazards (i.e., rocks, boulders, etc.) and by choosing a site free of such hazards. A variety of sensors and data processing algorithms are available for this purpose. All sensors and processing capabilities are on board the lander. For pinpoint landing, the determination of a safe landing site is made before descent begins (i.e., prior to atmospheric entry). The lander reaches this identified site and lands safely. All surface feature sensors (synthetic aperture radar (SAR), optical, etc.) and associated processing capabilities are carried by an imaging orbiter in an appropriate Mars orbit. For either of these options, an altimeter is required for accurate altitude measurements prior to final touchdown. The sensor issues and trades for targeting options have been addressed in Reference 4 and will not be repeated here.

For either of these options, the position and velocity of the lander with respect to the desired landing site must be determined. These landing site relative position and velocity estimates are input to the terminal descent guidance function. For purposes of analysis, navigated state position errors as a percentage of distance to the desired landing site of between 0.5% and 10% were assumed. For a 10 km initial altitude and up to 10 km required downrange translation, this range of error magnitudes corresponded to an initial navigated position accuracy of between 50 m and 1.5 km. The low end of this range corresponded to navigation capabilities for pinpoint landing while the high end of this range corresponded to navigation capabilities for hazard avoidance. Since the Robust E-Guidance law described below has a free parameter that can be adjusted to optimize descent performance in the presence of uncertainties, the performance of the guidance law can be optimized once the actual navigation strategy has been chosen and its accuracy has been assessed. The derivation of the REG guidance law is presented in the following section.

Guidance

The Robust E-Guidance (REG) algorithm is a derivative of the E-Guidance algorithms designed for use in the Apollo program [2][5]. This guidance algorithm essentially minimizes the integral of the square of the vehicle thrust acceleration subject to the terminal constraints of zero velocity and specified planet relative position. The REG algorithm differs from the original E-Guidance algorithms in that the effects of navigated state uncertainties, windshears, thrust level dispersions, and other off-nominal conditions are lumped together into a disturbance vector that is added to the state equations for position and velocity. The integral square thrust minimization is then performed in a minimax sense; i.e. the cost function is minimized over thrust and maximized over disturbance such that the resulting guidance strategy allows the vehicle to land safely in the presence of worst case disturbances. The optimal solution represents the saddle point of a linear quadratic differential game and can therefore be obtained through straightforward application of the calculus of variations.

The REG algorithm operates as follows. At each guidance update step (say every 0.1 seconds), the optimal thrust history for achieving a soft landing at the desired site is determined. The time variable t for the optimization problem is defined such that the current time is interpreted as $t = 0$. Therefore, the optimal thrust to be applied at the current time is determined as the value of the optimal thrust profile at $t = 0$.

The optimization problem uses the following equations of motion for a vehicle in the vicinity of the planet surface:

$$\frac{d\mathbf{x}}{dt} = \mathbf{v} \qquad \mathbf{x}(0) = \mathbf{x}_0 \tag{9}$$

$$\frac{d\mathbf{v}}{dt} = \mathbf{a} - \mathbf{g} + \mathbf{w} \qquad \mathbf{v}(0) = \mathbf{v}_0 \tag{10}$$

Here **x** and **v** are the lander position and velocity vectors with respect to the landing site, **a** is the thrust acceleration, **g** is the local gravity, and **w** is a vector that models the effects of possible uncertainties, disturbances and unmodeled dynamics (such as aerodynamic forces). The vectors **a** and **w** are unknown and are determined as part of

the optimization process. The cost function to be minimized by the thrust acceleration and maximized by the disturbance vector is

$$J = \frac{1}{2}\int_0^T \mathbf{a}^T\mathbf{a} - \gamma^2\, \mathbf{w}^T\mathbf{w}\; dt \tag{11}$$

subject to the constraints

$$\mathbf{x}(T) = \mathbf{x}_f \tag{12}$$

$$\mathbf{v}(T) = \mathbf{v}_f \tag{13}$$

where $\mathbf{x}_f$ and $\mathbf{v}_f$ are specified at the free final time T. Here γ is a weighting factor greater than zero chosen to limit the magnitude of the allowable dispersions (it is <u>not</u> a flight path angle). This problem is a linear two point boundary value problem and can be solved using the calculus of variations. Defining the Hamiltonian H to be

$$H = \frac{1}{2}\mathbf{a}^T\mathbf{a} - \frac{\gamma^2}{2}\mathbf{w}^T\mathbf{w} + \mathbf{P_x}^T\mathbf{v} + \mathbf{P_v}^T(\mathbf{a} - \mathbf{g} + \mathbf{w}) \tag{14}$$

the necessary conditions for optimality are given by

$$\frac{d\mathbf{P_x}}{dt} = -\frac{\partial H}{\partial \mathbf{x}} \tag{15}$$

$$\frac{d\mathbf{P_v}}{dt} = -\frac{\partial H}{\partial \mathbf{v}} \tag{16}$$

$$\frac{\partial H}{\partial \mathbf{a}} = 0 \tag{17}$$

$$\frac{\partial H}{\partial \mathbf{w}} = 0 \tag{18}$$

$$H(t = T) = 0 \tag{19}$$

Expressions (15) and (16) can be immediately integrated to give

$$\mathbf{P_x} = \mathbf{C_1} \tag{20}$$

$$\mathbf{P_v} = -\mathbf{C_1}\, t - \mathbf{C_2} \tag{21}$$

where $\mathbf{C_1}$ and $\mathbf{C_2}$ are vector constants to be determined. Expressions (17) and (18) can be solved for **a** and **w** to yield

$$\mathbf{a} = -\mathbf{P_v} \tag{22}$$

$$\mathbf{w} = \frac{1}{\gamma^2}\mathbf{P_v} \tag{23}$$

These expressions can be used to solve the equations of motion for the terminal states $\mathbf{x_f}$ and $\mathbf{v_f}$:

$$\mathbf{x_f} = \mathbf{x_0} + \mathbf{v_0}\,T + (1 - \frac{1}{\gamma^2})\,(\mathbf{C_1}\,\frac{T^3}{6} + \mathbf{C_2}\,\frac{T^2}{2}) - \frac{1}{2}\mathbf{g}\,T^2 \tag{24}$$

$$\mathbf{v_f} = \mathbf{v_0} + (1 - \frac{1}{\gamma^2})\,(\mathbf{C_1}\,\frac{T^2}{2} + \mathbf{C_2}\,T) - \mathbf{g}\,T \tag{25}$$

Since the desired terminal conditions $\mathbf{x_f}$ and $\mathbf{v_f}$ are known, expressions (24) and (25) constitute a set of linear algebraic equations for the constants $\mathbf{C_1}$ and $\mathbf{C_2}$ in terms of the unknown final time T. Solving (24) and (25) for $\mathbf{C_1}$ and $\mathbf{C_2}$ yields

$$\mathbf{C_1} = \frac{6\,(\mathbf{v_f} + \mathbf{v_0})T - 12\,(\mathbf{x_f} - \mathbf{x_0})}{\kappa T^3} \tag{26}$$

$$\mathbf{C_2} = \frac{6\,(\mathbf{x_f} - \mathbf{x_0}) - 2\,(\mathbf{v_f} + 2\mathbf{v_0})\,T + \mathbf{g}T^2}{\kappa T^2} \tag{27}$$

where κ is defined as $\kappa = 1 - 1/\gamma^2$. The final time T can be determined by using (19), which states that the value of the Hamiltonian at t=T must be zero. Substituting (20)-(23) and (26)-(27) into the expression (14) for the Hamiltonian yields the following quartic polynomial in the final time T:

$$A\,T^4 + B\,T^2 + C\,T + D = 0 \tag{28}$$

where

$$A = -\mathbf{g}^T\mathbf{g} \tag{29}$$

$$B = \beta^T\beta - 12\,\mathbf{v_f}^2 - 12\,\mathbf{v_0}^T\mathbf{v_f} \tag{30}$$

$$C = 2\,\alpha^T\beta + 24\,(\mathbf{x_f} - \mathbf{x_0})\,\mathbf{v_f} \tag{31}$$

$$D = \alpha^T\alpha \tag{32}$$

$$\alpha = 6\,(\mathbf{x_0} - \mathbf{x_f}) \tag{33}$$

$$\beta = 2\,(\mathbf{v_0} + 2\mathbf{v_f}) \tag{34}$$

The roots of (28) can be determined through an analytical procedure presented in Reference 6. Typically, two of the four roots are a complex conjugate pair and one of the two remaining real roots is negative. The one real and positive root is the desired value for the final time T.

Once T has been determined, the optimal thrust profile is given by

$$\mathbf{a} = \mathbf{C_1}\, t + \mathbf{C_2} \tag{35}$$

with $\mathbf{C_1}$ and $\mathbf{C_2}$ determined from (26)-(27). Since the guidance law assumes that the current time is the initial time t = 0, the optimal thrust at the current time is given by

$$\mathbf{a} = \mathbf{C_2} \tag{36}$$

Using (27) for $\mathbf{C_2}$ yields the final expression for the optimal thrust

$$\mathbf{a} = \frac{6\,(\mathbf{x}_f - \mathbf{x}_0) - 2\,(\mathbf{v}_f + 2\mathbf{v}_0)\,T + \mathbf{g}T^2}{\kappa T^2} \tag{37}$$

The descent vehicle is guided to a soft landing at the desired site by aligning the thrust vector of the descent engine with the commanded acceleration vector **a** and by commanding a thrust $\mathbf{F}_{th}$ of

$$\mathbf{F}_{th} = m\,\mathbf{a} \tag{38}$$

where m is the flight software estimate of the current vehicle mass.

The expression for the worst case disturbance vector can be similarly determined as

$$\mathbf{w} = -\frac{6\,(\mathbf{x}_f - \mathbf{x}_0) - 2\,(\mathbf{v}_f + 2\mathbf{v}_0)\,T + \mathbf{g}T^2}{\gamma^2\,\kappa T^2} \tag{39}$$

While this quantity does not need to be calculated on board, it can be compared with the magnitude of expected disturbances in order for the designer to properly size the value of the design parameter γ. Note that as $\gamma \to \infty$, $\mathbf{w} \to 0$ and $\kappa \to 1$. As such, this guidance law reduces to E-Guidance in the limit as $\gamma \to \infty$.

The REG law uses the expression (37) for **a** at regular intervals (every 0.1 seconds) along the descent trajectory to calculate the thrust acceleration commands to be issued. The actual dispersions encountered will probably not be equal to the worst case disturbances given by expression (39), but this fact will only improve the performance of the algorithm.

Guidance Law Performance

The performance of the guidance algorithm was assessed through a nonlinear numerical simulation that included the effects of aerodynamics and navigated state uncertainties. The design parameter γ was adjusted until a satisfactory combination of ΔV expenditure and terminal accuracy was achieved. The performance results were also compared with those from the standard E-Guidance algorithm.

The performance of the guidance algorithm during actual flight will be affected by a number of error sources, including navigated position and velocity errors, landing site redesignation, thrust offsets, surface winds, etc. In order to simplify the evaluation of guidance law performance, the performance was evaluated in the presence of two sources of uncertainty: a) landing site redesignation during descent and b) navigated state position errors for descent to a predesignated site. Other sources of error are expected to yield results similar to those presented below. For all cases, the lander's physical properties were those presented in Table 13. Note that only the throttleable engines were used for descent. Performance analyses for each of these error sources are presented in the following paragraphs.

Landing Site Redesignation. A representative scenario was selected for testing guidance law performance with low altitude landing site redesignation. The lander was assumed to start 10 km above the planet surface, descending vertically at 120 m/s. The original landing site was located directly beneath the lander, i.e. at zero downrange translation distance. As soon as the lander descended below an altitude of 2 km, the landing site was redesignated to be a specified distance downrange. Distances of 500 m to 5 km were examined.

Results for ΔV expenditures and touchdown velocities were obtained for $\gamma = \infty$ and $\gamma = 4$ for each downrange translation distance. The case where $\gamma = \infty$ corresponds to the standard E-Guidance method, while the choice of $\gamma = 4$ was made after iterating several times on the simulation results. The results for touchdown velocity versus required translation distance are presented in Figure 34. Note that for E-Guidance, the vehicle could not translate downrange more than 2.3 km without crashing (the touchdown velocities became quite large). However, for REG the lander touched down safely (touchdown velocity < 0.5 m/s) for translation distances as large as 5 km. Therefore, the range of the vehicle was greatly enhanced through the use of REG. The ΔV requirements for both guidance laws are shown in Figure 35. Note that the ΔV requirements for REG are 10-20 m/s higher than those for E-Guidance for translation distances up to 2.3 km. For larger translation distances, the ΔV requirements for E-Guidance are basically meaningless since the vehicle crashes for these translation distances. Evidently, the extra robustness offered by REG comes at the expense of slightly higher fuel consumption.

Navigated Position Uncertainty. A set of representative test cases was selected in order to evaluate the performance in the presence of various levels of target relative navigated position uncertainty. For each case the lander was assumed to start 10 km above the planet surface, descending vertically at 120 m/s. Several target landing sites were examined ranging from 1 km downrange to 6 km downrange. All landing sites were located at zero altitude. Information regarding the range to the landing site was assumed to be available to an accuracy that was varied from one simulation run to the next. Navigation error magnitudes of 0%, 0.5%, 1%, 2.5%, 5%, and 10% were examined.

Results for ΔV expenditures and touchdown velocity were obtained for $\gamma = \infty$ and $\gamma = 4$ for each level of navigated state error for each landing site. The results for touchdown velocity versus range error magnitude for each landing site are presented

in Figures 36 through 38. For the landing site at 6 km, the terminal velocities for both guidance laws are within acceptable limits. However, for the landing site at 1 km, the touchdown velocity for the E-Guidance law reaches unacceptably high levels as the range error is increased. The REG law, however, gives touchdown velocities of less than 0.5 m/s for any level of range uncertainty up to 10%. For this particular situation, the use of REG over standard E-Guidance resulted in the difference between mission success and mission failure for a soft landing mission. The ΔV expenditures for $\gamma = \infty$ and $\gamma = 4$ for the 1 km downrange case are shown in Figure 39. Note that the ΔV requirements for REG are 20 to 40 m/s higher than for E-Guidance. The extra robustness offered by REG comes at the expense of slightly higher fuel consumption, although the difference amounts to less than 8%.

Discussion

The reason that the standard E-Guidance algorithm allowed such high touchdown velocities for certain cases is that the error sources caused the commanded thrust magnitude to exceed the maximum thrust capability of the descent engines. Other sources of error are expected to have a similar effect on performance. The use of REG resulted in a solution with a slightly longer time of flight and a slightly slower increase in thrust level with time, so the maximum engine thrust level was not exceeded. Of course, some of the difficulties with E-Guidance could be avoided by increasing the time of flight over that calculated from the condition (19) or (28). For example, the time of flight found from (28) could be simply multiplied by some number greater than 1.0. The problem with this approach is that it increases the required fuel consumption to the same level as that of REG without providing either a) a time of flight calculation based explicitly on optimization considerations, or b) information concerning the disturbance levels for which the algorithm will still yield acceptable performance. The use of REG, on the other hand, yields a) an explicit expression (28) for time of flight based on the necessary condition for optimality (19), and b) an analytical expression for the worst case disturbance vector $\mathbf{w}$. The use of REG therefore provides a mathematically justifiable technique for extending the final time (thereby reducing peak thrust values) while providing an explicit calculation of the magnitude of worst case disturbances for which the guidance law will still yield acceptable performance (i.e. a safe landing). Note that the magnitude of $\mathbf{w}$ can be compared with the expected trajectory disturbances, and γ can be varied until the magnitude of $\mathbf{w}$ (as determined from (39)) encompasses the worst case disturbances expected during actual flight.

The ΔV requirements for terminal descent and translation over distances up to 10 km were also examined. Only the REG law for $\gamma = 4$ was used, since the ΔV requirements were obtained primarily for vehicle sizing considerations. ΔV requirements were obtained under the assumtion of zero range estimation error, since this case results in the highest ΔV expenditures. The results are presented in Figure 40. Note that ΔV requirements ranged from 505 m/s for zero required translation distance to 677 m/s for 10 km required translation distance. These results are quite close to preliminary estimates for optimal descent ΔV requirements as determined in Reference 1.

Table 13. Lander Physical Properties

Parameter	Value	Units
Initial mass	2500	kg
Drag coefficient	1	–
Aerodynamic reference area	16.4	m^2
Main engine		
Thrust	16680	N
Isp	343	sec
Throttleable engines (total)		
Thrust	15560	N
Isp	304	sec

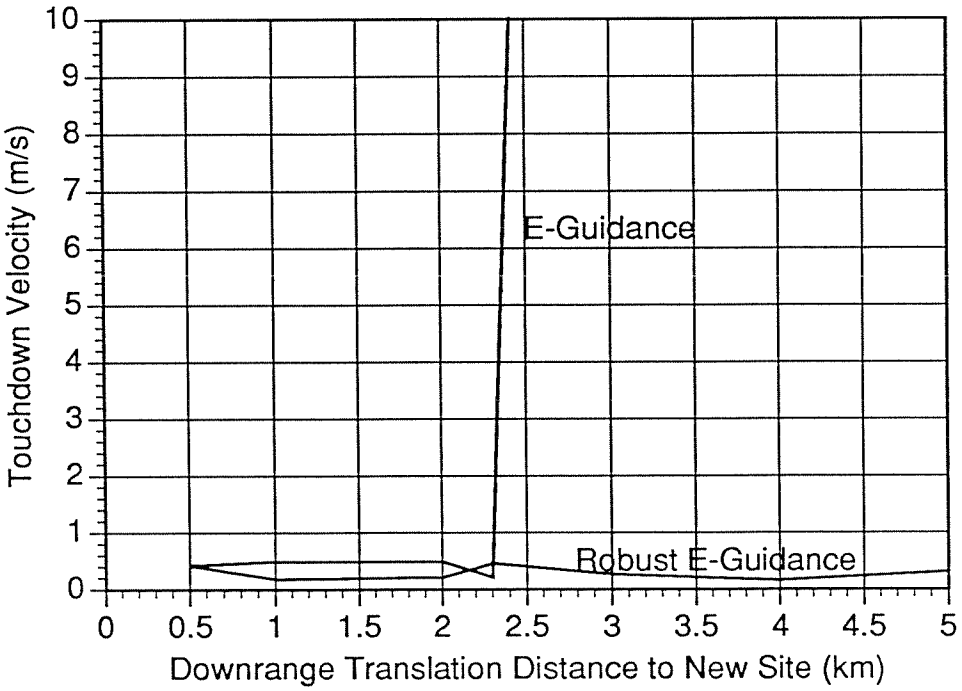

Figure 34. Touchdown Velocity Versus Downrange Distance for Redesignated Landing Site

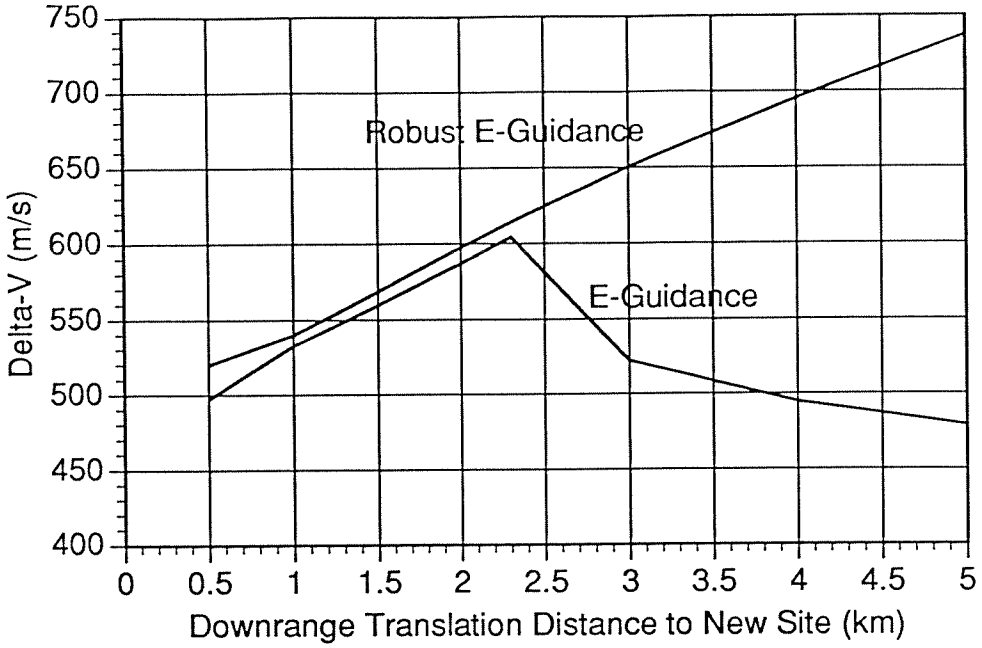

Figure 35. ΔV Required Versus Downrange Distance for Redesignated Landing Site

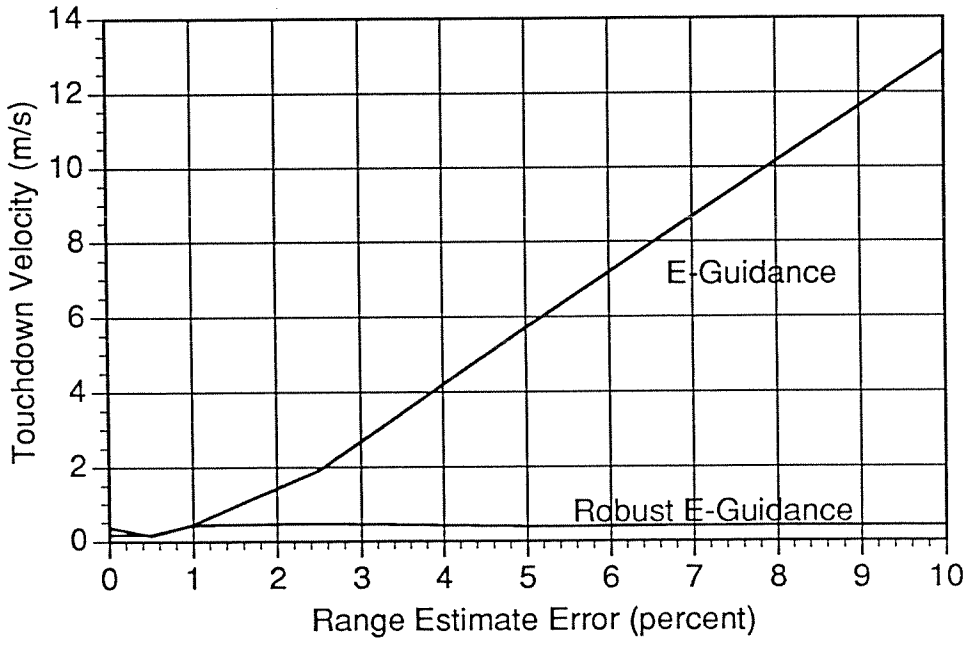

Figure 36. Touchdown Velocity Versus Error in Estimated Range, Landing Site at 1 km Downrange

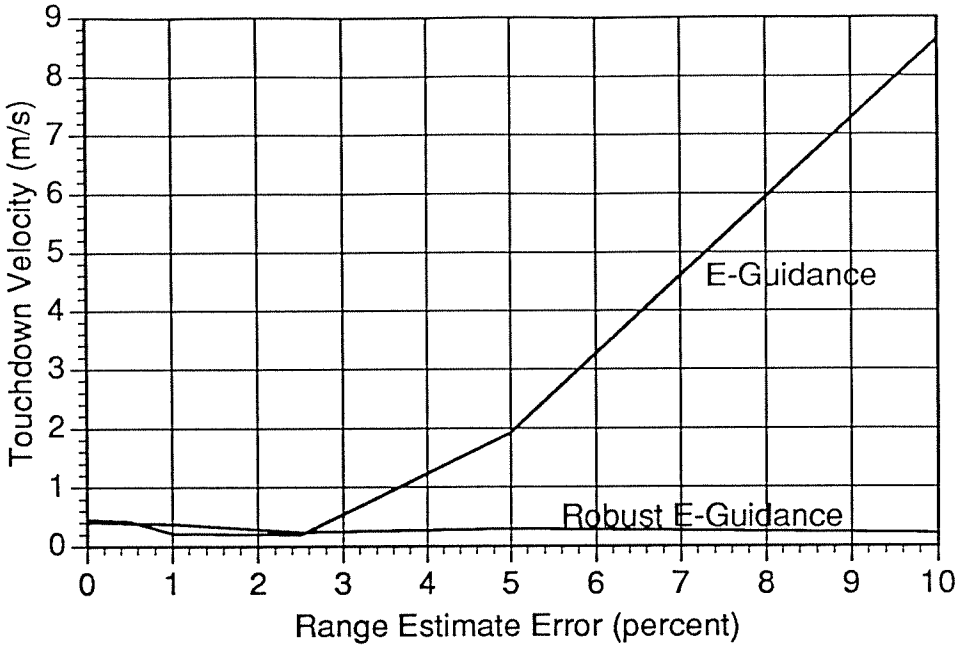

Figure 37. Touchdown Velocity Versus Error in Estimated Range, Landing Site at 3 km Downrange

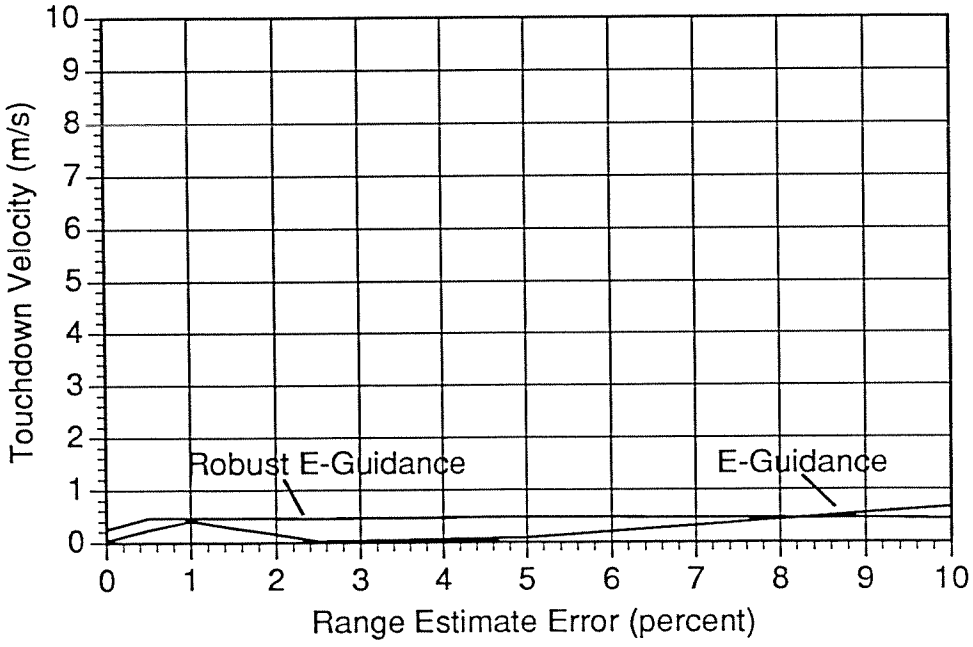

Figure 38. Touchdown Velocity Versus Error in Estimated Range, Landing Site at 6 km Downrange

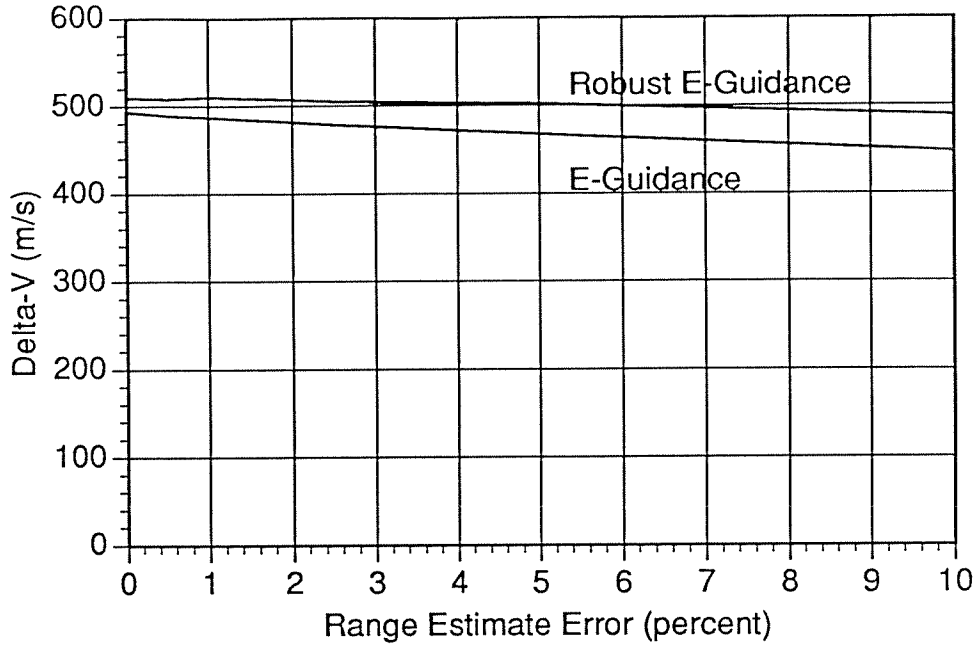

Figure 39. ΔV Required Versus Error in Estimated Range

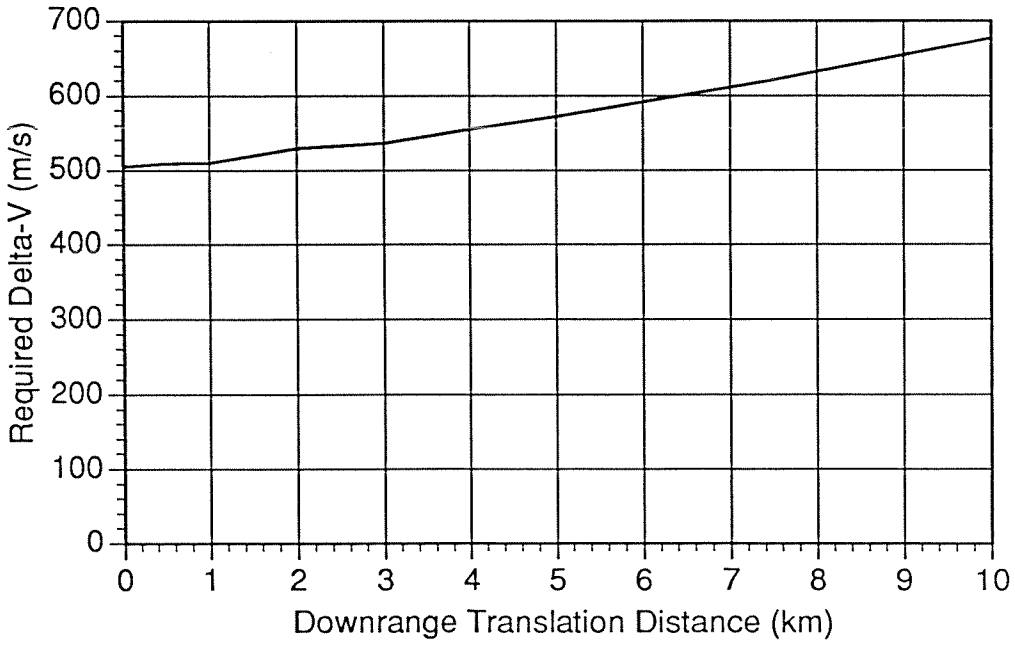

Figure 40. ΔV Required Versus Translation Distance

SUMMARY

1. The ballistic aerobrake entry concept exceeds the performance capability of an aeromaneuvering system at Mars and offers a much simpler entry-to-landing approach.

2. The aeromaneuvering concept meets the mission requirements, but encounters a demanding aerodynamic requirement for terminal aerodynamic deceleration (i.e., parachute deployment).

3. A new guidance law, Robust E-Guidance, has been developed to provide more robustness to the propulsive terminal descent phase while retaining near fuel optimal performance. This guidance law extends the safe landing range of the vehicle over that of E-Guidance while requiring a minimal increase in ΔV expenditures (5-8%) over the E-Guidance law.

ACKNOWLEDGEMENT

The research and development described in this publication was carried out, in part, by the TRW Space and Technology Group, Redondo Beach, California, under NASA Contract NAS9-18141. The authors would like to express their thanks to the following people who provided considerable technical insight and assistance to the authors: P. Adamsen, W. F. Balmanno, R. Colbert, J. Crawford, W. Koerner, D. Post, T. Shivananda, D. Stager, R. Wilkinson.

REFERENCE

1. "Mars Rover Sample Return (MRSR) Delivery and Return Study", TRW Report No. NAS 9-18141, Phase A Study performed for NASA Johnson Space Flight Center, June, 1990.
2. G. W. Cherry, "A Unified Explicit Technique for Performing Orbital Insertion, Soft Landing, and Rendezvous with a Throttleable Rocket-Propelled Space Vehicle," AIAA Guidance and Control Conference, Cambridge, Mass., August 1963.
3. M. I. Cruz, "Trajectory Optimization and Closed Loop Guidance of Aeroassisted Orbital Transfer," AAS Paper 83-413, AAS/AIAA Astrodynamics Specialist Conference, Lake Placid, N.Y., August 1983.
4. J. Stevenson, T. Morrison, and T. Murphy, "Autonomous Landing on Mars," AAS Paper 90-050, 13th AAS Guidance and Control Conference, Keystone, Colorado 1990.
5. L. E. Adkins, A. A. Dzilvelis, D. F. McAllister, A. J. Taylor, "Automatic Lunar Landing Guidance Performance Analysis Study", TRW Document 2224-6011-R0000, 22 June 1966.
6. CRC Standard Mathematical Tables, 26th Edition, CRC Press, Boca Raton, Florida, 1981.